We are IntechOpen, the world's leading publisher of Open Access books Built by scientists, for scientists

4,800
Open access books available

122,000
International authors and editors

135M
Downloads

Our authors are among the

154
Countries delivered to

TOP 1%
most cited scientists

12.2%
Contributors from top 500 universities

CLARIVATE ANALYTICS BOOK CITATION INDEX INDEXED

WEB OF SCIENCE™

Selection of our books indexed in the Book Citation Index in Web of Science™ Core Collection (BKCI)

Interested in publishing with us?
Contact book.department@intechopen.com

Numbers displayed above are based on latest data collected.
For more information visit www.intechopen.com

Chapter 10

Preparation of Nickel-Based Nanolubricants and Investigation of their Tribological Behavior

Yujuan Zhang, Shengmao Zhang, Pingyu Zhang, Guangbin Yang and Zhijun Zhang

Additional information is available at the end of the chapter

http://dx.doi.org/10.5772/64592

Abstract

In situ surface-modification technique is adopted in present research to fabricate a series of Ni nanoparticles as well as Cu@Ni nanoparticles with different size and morphology. The correlation among the composition, structure, size, and morphology and tribological properties of as-synthesized additives were explored, and the friction-reducing, antiwear, and worn surface self-healing mechanisms of the additives were discussed. It was found that Ni nanoparticles with a smaller size show higher surface activity and can readily deposit on the sliding surface and form a stable and continuous protective layer thereon. Compared with sphere-like and triangular rod-like Ni nanoparticles, triangular plate-like Ni nanoparticles are more liable to form protective layer. Compared to Ni-based nanolubricants, as-synthesized Cu@Ni nanolubricants exhibit better friction-reducing, antiwear, and extreme pressure properties. It is because the highly active Ni nanocores and O- and N-containing organic modifying agents can readily form boundary lubricating film on sliding steel surfaces, while Cu nanocores can easily deposit on sliding steel surface to form a protective layer (self-healing film) thereon. Ni nanoparticles as nanoadditives in solid-liquid lubricating system significantly reduce the friction in all lubrication regimes: As a nanolubricant, Ni nanoparticles exhibit popular and effective friction-reducing, antiwear, and extreme pressure properties.

Keywords: nickel nanoparticles, Cu@Ni nanolubricant, DLC-Ni solid liquid composite lubrication system, preparation, tribological behavior

1. Introduction

Recently, nanoparticles used as lubricant additives have received increased attention because of their excellent antiwear and friction-reducing properties [1, 2]. Several tribological mechanisms of nanolubricants have been proposed such as deposited film, surface alloying, cold welding, and rolling effect [3–7]. It has been well recognized that tribological properties of nanoparticles can be affected by their chemical composition, particle size, and morphology, in which, however, the exact tribological mechanisms of nanolubricants still remain unknown. On the other hand, their application in the field of tribology is still hindered by their poor dispersibility because of their high surface energy and activity leading to agglomeration in lubricant base oils. Therefore, it is vital to improve the dispersion capacity of nanoparticles in base oil through *in situ* surface modification with a variety of organic molecules [1, 2]. Compared with the *in situ* surface-modification technology established in the early 1990s [3, 7–14], current surface-modification technique for nanolubricants is inconvenient and less cost-effective, which involves several steps including synthesis of nanoparticles and follow-up dispersion of nanoparticles in lubricant base oils. In order to overcome the low productivity of nanoparticles and the difficultly in storing and dispersing the nanoparticles, it becomes significant to develop one-step method for preparing *in situ* surface-capped nanolubricants so as to promote their industrialization.

Unfortunately, current synthetic approaches for Ni nanoparticles with controllable size and shape are usually complicated and need to use a large number of solvents, such as polyol synthesis [15], electrochemical reduction [16], microwave heating, reduction of organometallic precursors [17–19], and thermal decomposition of organic complexes [20–22]. More badly, even after surface modification with organic molecules, currently available Ni-based nanolubricants are still liable to aggregate and can hardly be monodispersed in lubricant base oil [23, 24]. On the other hand, it was more ideal to study the relationship between particle size, morphology of metal nanolubricants, and its tribological mechanism through one kind of metal nanoparticle.

In this chapter, a facile *in situ* one-step thermal decomposition route is used to prepare size and morphology-controllable monodispersed Ni nanoparticles with a narrow size distribution, which can be dispersed in PAO6 base oil and used as nickel-based nanolubricants directly. The tribological properties of Ni nanolubricants in base oil demonstrated strong dependence on the size, morphology, and composition. Meanwhile, the Ni nanoparticle significantly reduces the friction of diamond-like carbon (DLC)/di-iso-octyl sebacate (DIOS) liquid-solid composite lubricating system in all lubrication regimes: boundary, mixed, and elasto-hydrodynamic lubrication. This *in situ* one-step thermal decomposition route probabilizes popular, effective antiwear and friction-reducing properties by applying Ni-based nanolubricants.

2. The effect of size of Ni nanolubricant on its tribological properties

The chemical reaction for *in situ* preparation of Ni nanoparticles is expressed in **Figure 1**. OAM(oleylamine) is a lot in comparison to nickel, but actually, OAM is not only coordination

http://dx.doi.org/10.5772/64592

ligand of nickel acetate by amidocyanogen in early solution, but also reducing agent and surface-capping agent for Ni nanoparticles. Upon completion of the reaction, decomposition byproducts of $Ni(HCOO)_2 \cdot 2H_2O$ are evaporated under a current of inert gas at high temperature and only surface-capped Ni nanoparticles by oleylamine and oleic acid remain in PAO6 base oil, and excess oleylamine and oleic acid in PAO6 do not matter because these are also lubricant additives, so nickel-based nanolubricants are obtained directly by this *in situ* one-step route. This should be critical to the tribological application of nickel-based nanolubricants. As shown in **Figure 2**, there are three characteristic peaks at 44.5°, 51.8°, and 76.4° appearing in the XRD patterns of Ni nanoparticles with different sizes. The three peaks can be assigned to the diffractions of (111), (200), and (220) crystal planes of pure face-centered cubic (FCC) Ni (JCDPS No.7440-02-0). The diffraction peaks are significantly broadened, which indicates that the crystalline size of Ni nanoparticles is very small.

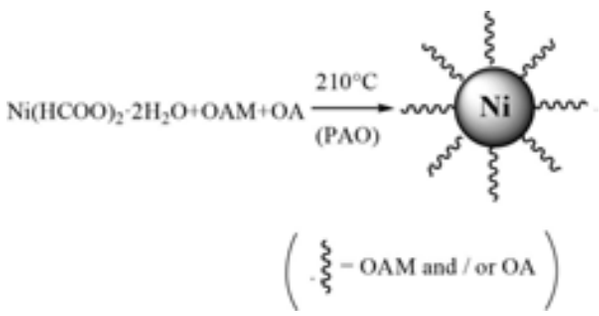

Figure 1. Chemical reaction for preparing Ni nanoparticles.

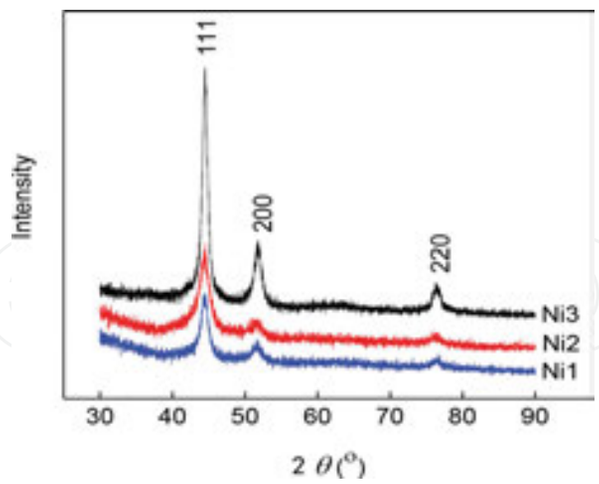

Figure 2. XRD patterns of Ni nanoparticles with different size.

The TEM images of Ni nanoparticles with different size as well as the size distribution are shown in **Figure 3**. It can be seen that Ni nanoparticles have sphere-like morphology, and through varying dosage of PAO6 from 80 to 40 and 20 mL their average diameter is tunable from about 7.5 to 13.5 and 28.5 nm. As-synthesized Ni nanoparticles show no sign of obvious

aggregation. It can be deduced that the nucleation and growth process of Ni nanocrystalline can be adjusted by OAM and OA through controlling chemical reaction driving force and affording monodispersed Ni nanoparticles with different sizes. The simultaneous presence and relative amounts of binary modifiers OAM and OA are paramount. OAM is the reductant and at the same time controls the nucleation rate. OA as an efficient surface-modification agent are favorable for probing capping mechanism and affording size-tunable monodispersed Ni nanoparticles. As is the experimental result, the higher ligands concentrations led to the formation of the particles with larger sizes, because the higher the concentration of the ligands, the lower the monomer reactivity would be; therefore, there would be fewer nucleuses formed and resulted in larger nanoparticles [25, 26].

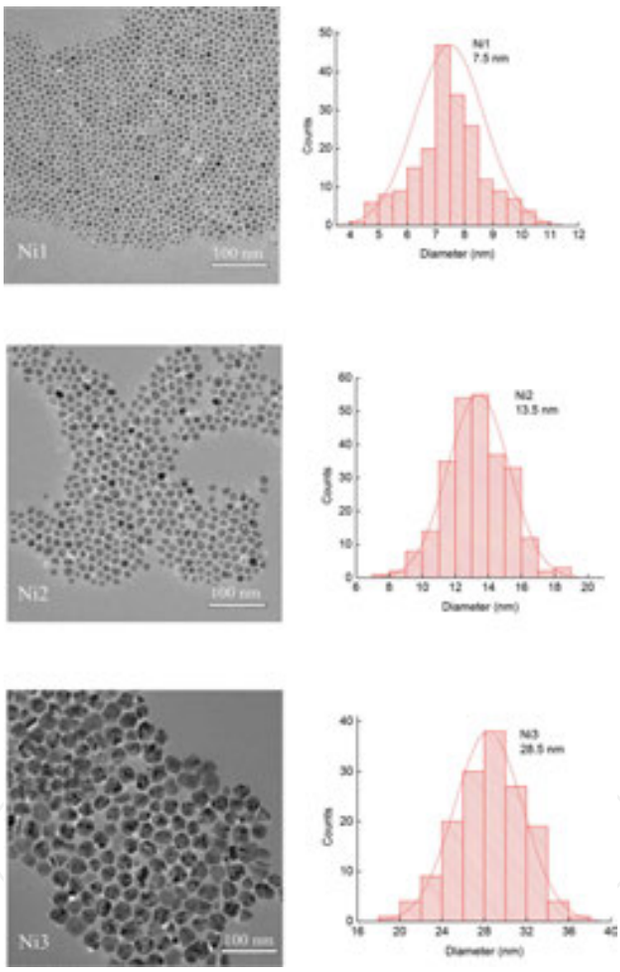

Figure 3. TEM images and size distribution of surface-capped Ni nanoparticles with different size.

Figure 4 shows the optical picture of the nickel nanoparticles in PAO6 after a month. The results indicate that the nickel nanoparticles are still equably distributed in PAO6 after a month and there is no obvious agglomeration behavior, which fits in quite with the TEM analysis.

FTIR(Fourier transform infrared spectrometer) analysis was conducted to study the interaction between organic surface modifier and Ni nanocore. As shown in **Figure 5**, the characteristic

http://dx.doi.org/10.5772/64592

absorption bands of pure OA at 1711 and 939 cm^{-1} correspond to the stretching vibrations of C═O and the bending vibration of ─OH of carboxyl group. As to pure OAM, the characteristic absorption bands of amine group at 3367 and 3295 cm^{-1} can be assigned to the symmetric and asymmetric stretching vibrations of primary amine N─H, the peak at 1583 cm^{-1} can be assigned to the scissoring mode of ─NH_2, and the one at 967 cm^{-1} can be assigned to the bending vibration mode of ─NH_2 [27]. The characteristic peaks of oleic group at 2922 and 2852 cm^{-1} appeared in both pure OAM and OA, the bending vibration mode of C─H at 1464 cm^{-1}, and the methylene rocking vibration of a minimum of four methyl groups ($(CH_2)_4$) in the 720 cm^{-1} region [28]. As to surface-modified Ni nanoparticles, the presence of OAM and OA as capping agents on the surface are confirmed by the characteristic peaks of oleic group at 2922, 2852, 1464, and 720 cm^{-1}. However, surface-capped Ni nanoparticles do not show the signal of primary amino group at 3367, 3295, 1583, and 967 cm^{-1} and the signal of free carboxyl group at 1711 and 939 cm^{-1}, at the same time some new absorption peaks of asymmetric and symmetric stretching vibrations of ─COO─ at 1543 and 1460 cm^{-1} and stretching vibration of C─N at 1071 cm^{-1} appeared, which indicates that two oxygen atoms in OA are symmetrically coordinated to the surface of Ni nanocore, and the OA chain is attached in a bidendate mode [29]. Therefore, it can be deduced that the organic surface modifiers OAM and OA chemically bond on the surface of Ni nanoparticles that prevents nanoparticles from oxidation and aggregation, which improved their compatibility with lubricating base stocks.

Figure 4. Picture of the nickel nanoparticles in PAO6 after a month.

TGA/DTA curves of surfaced-modified Ni nanoparticles are shown in **Figure 6**. As-synthesized Ni nanoparticles lose about 10% weight in the temperature range of 28~500°C. Within 28~250°C the slow weight loss corresponds to the volatilization of a small amount of OAM and OA physically adsorbed on the surface of Ni particles. Around 256°C the rapid weight loss is due to the decomposition of chemically adsorbed OAM and OA. Over 566°C the weight loss can be due to the elimination of decomposed residuals [30]. At the same time, in the DTA curve the exothermic peak around 271°C is due to the thermal decomposition of organic modification layer. It can be deduced that OAM and OA chemically bonded with Ni nanocores favor to improve the thermal stability of Ni nanoparticles.

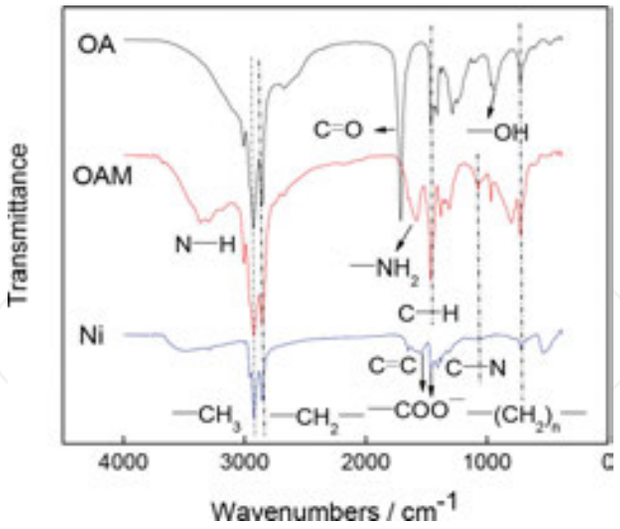

Figure 5. FTIR spectra of OA, OAM, and as-separated Ni nanoparticles.

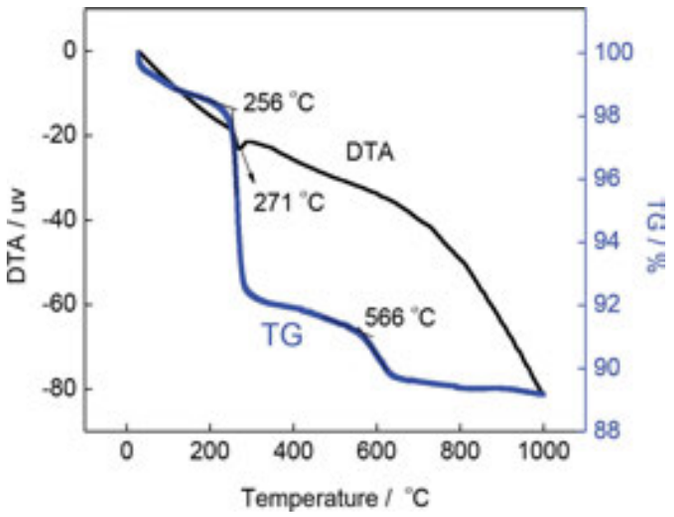

Figure 6. TG-DTA curves of as-separated Ni nanoparticles.

The variation of coefficient of friction (COF) (a) and wear scar diameter (WSD) (b) with the concentration of Ni nanoparticles in PAO6 are shown in **Figure 7** (four-ball friction and wear tester, load 300 N, rotary speed 1450 rpm, duration 30 min; for a comparison the data for PAO6 containing modifier are also given). It can be seen that the friction coefficient increases slightly with different Ni nanoparticles size and the surface-modifying agents, but the antiwear ability of base stock PAO6 is significantly improved. Moreover, their size and concentration is closely related with the antiwear ability of Ni nanoparticles in PAO6. At the additive concentration of 0.05% (mass fraction), sample Ni1 with smaller average diameter is more effective than samples Ni2 and Ni3 in reducing WSD of the steel-steel contact. It is consistent with the well-known Hall-Petch effect and Archard's law, which is mostly used in adhesion and abrasive wear conditions [31]. Besides, direct contact between the sliding steel surfaces can be avoided by the

http://dx.doi.org/10.5772/64592

deposition and/or adsorption films of surface-modified Ni nanoparticle on rubbed steel surfaces thereby retarding adhesion wear and increasing the antiwear ability of PAO6 base oil.

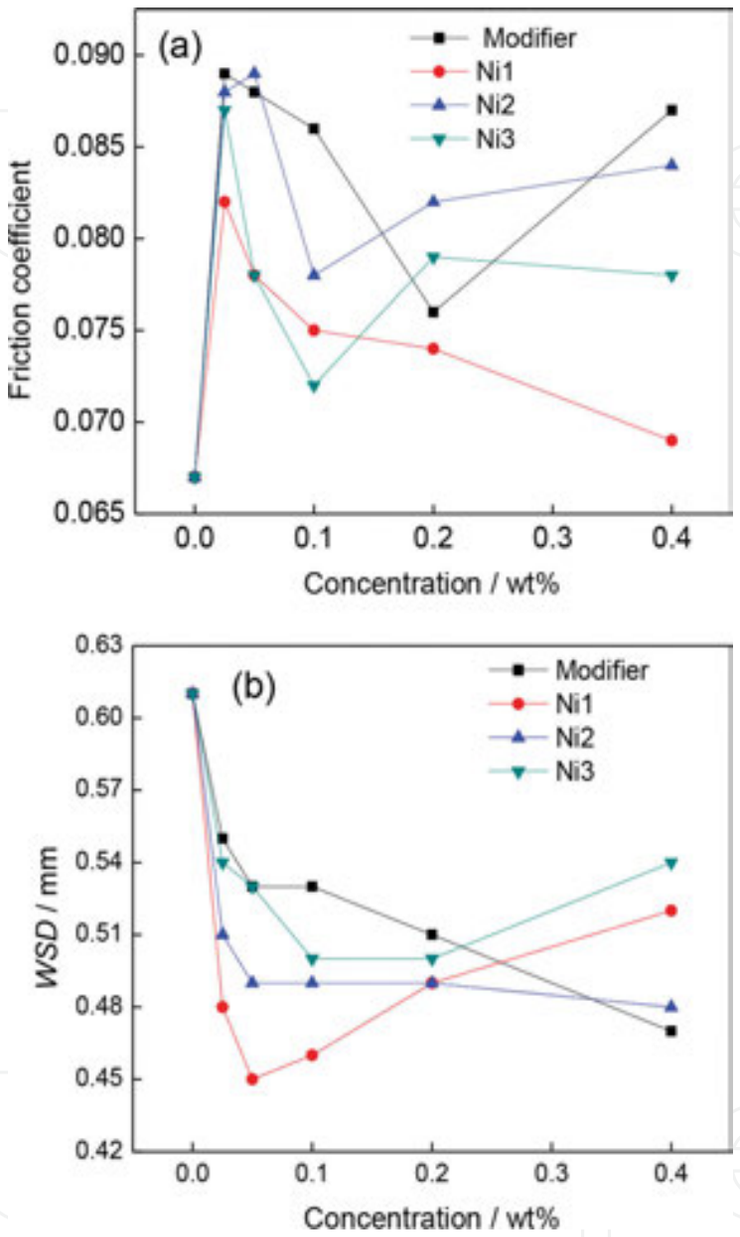

Figure 7. Variation of COF (a) and WSD (b) with the concentration of Ni nanoparticles.

The COF and WSD as functions of load under the lubrication of PAO6, PAO6 + modifier, and PAO + 0.05% Ni nanoparticles are shown in **Figure 8**. It can be seen that with rising load the COF decreases initially and increases later, and WSD increases monotonously therewith. Besides, under lower load, the applied force concentrates on a small number of large particles, which results in a higher friction coefficient owing to severe abrasion. Under higher load, large nanoparticles will undergo deformation, which leads to an even distribution of applied force on contact area thereby reducing COF. Besides, Ni nanoparticles with smaller size can improve

the antiwear ability of PAO6 base oil, possibly because they are more easily chemically adsorbed on steel sliding surfaces to form boundary lubricating films.

Figure 9 shows the P_B and P_D values of various lubricant systems. PAO6 doped by Ni nanoparticles with different size has a higher P_B value than PAO6 and PAO6 + surface modifiers, and the P_B value of the lubricants is irrelevant to the size of the Ni nanoparticles. It can be deduced that Ni nanoparticles are able to improve the load-carrying capacity of PAO6.

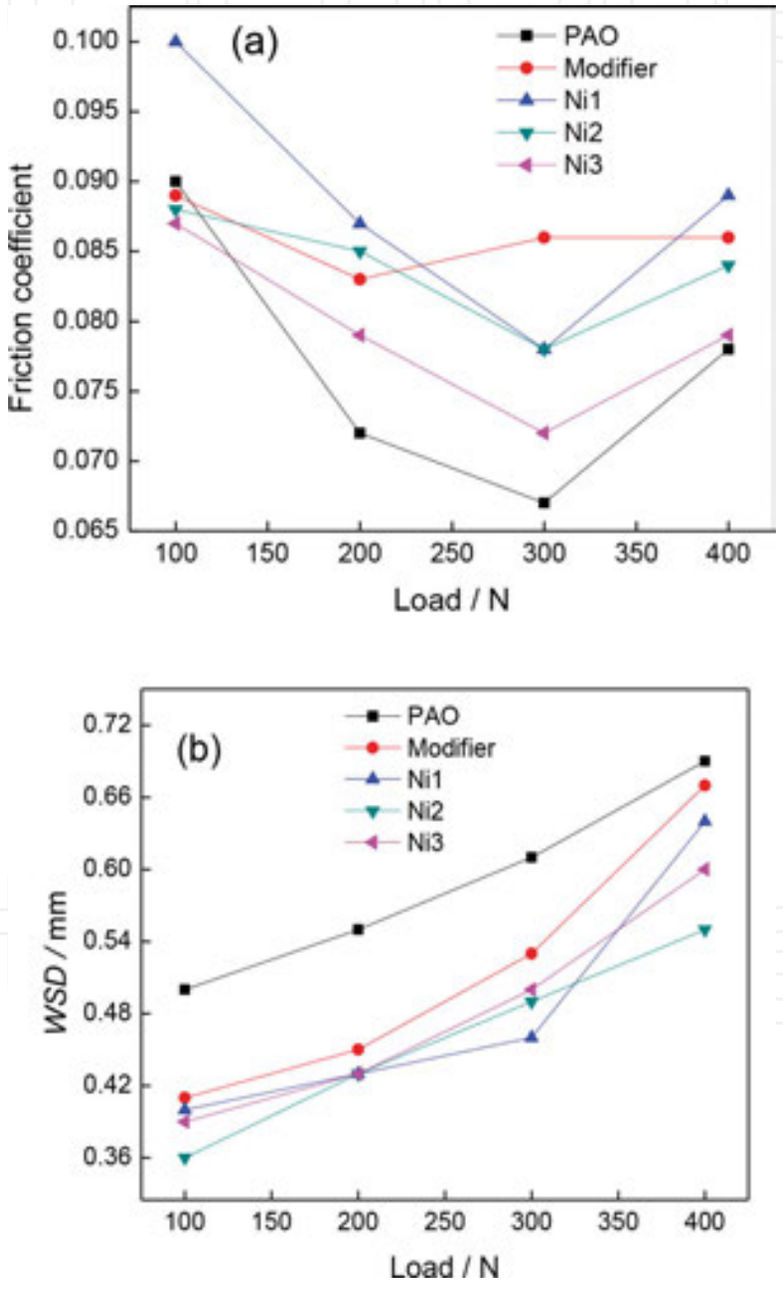

Figure 8. Friction coefficient (a) and wear scar diameter (b) versus applied load under the lubrication of PAO6, PAO6 + surface-modifiers, and nanolubricants containing 0.05% Ni nanoparticles with different size (four-ball friction and wear tester, 1450 rpm, 30 minutes).

http://dx.doi.org/10.5772/64592

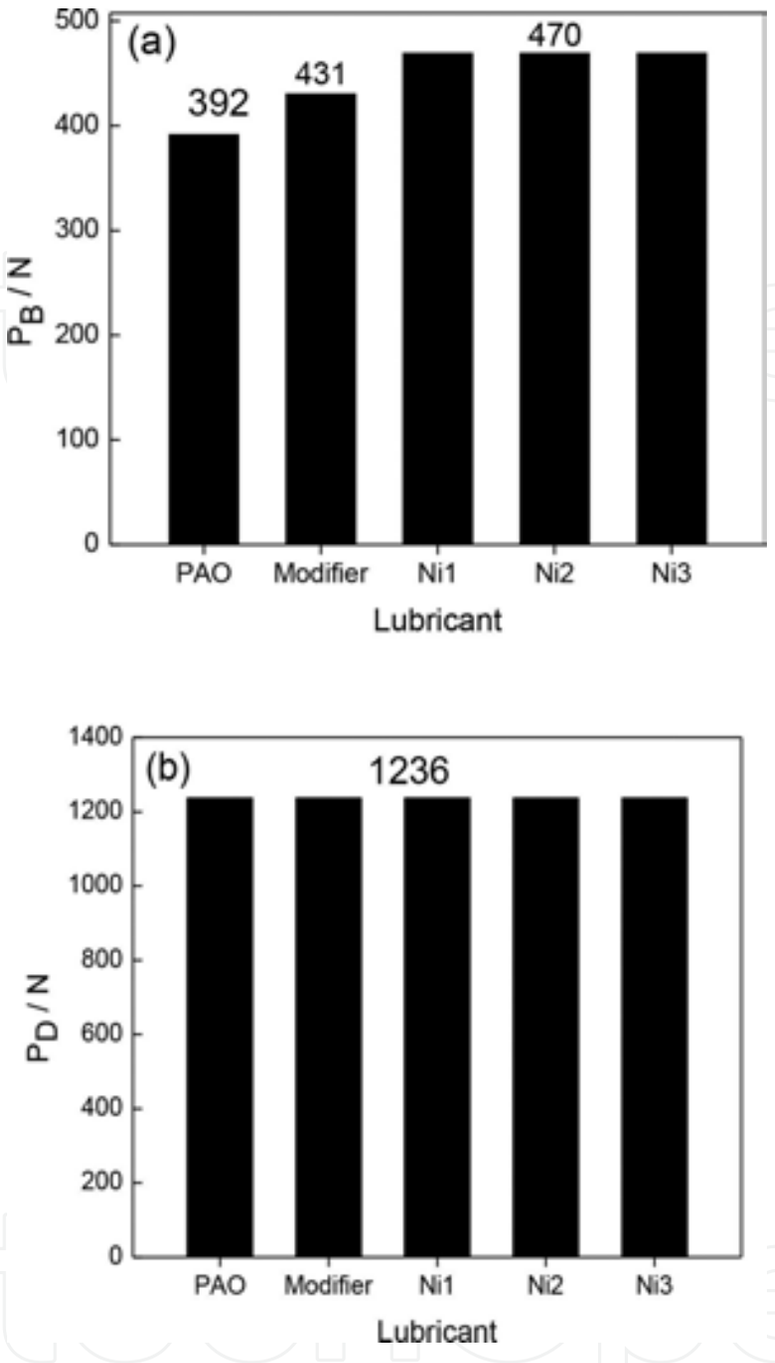

Figure 9. P_B(a) and P_D(b) values of various lubricant systems (four-ball friction and wear tester, 1450 rpm, 300 N).

SEM images of worn surfaces on steel balls lubricated by various lubricant systems are shown in **Figure 10**. It can be seen that the WSD of steel balls lubricated by PAO6 + Ni nanoparticles is smaller than that lubricated by pure PAO. Particularly, the smallest WSD is obtained under the lubrication of PAO6 + Ni1. Compared with PAO6 + Ni2 or PAO6 + Ni3, the worn surface on the steel ball lubricated by PAO6 + Ni1 is smooth and shows only shallow scratch grooves, which well conforms to the better antiwear ability of nanolubricants with smaller Ni nanoparticles (Ni1).

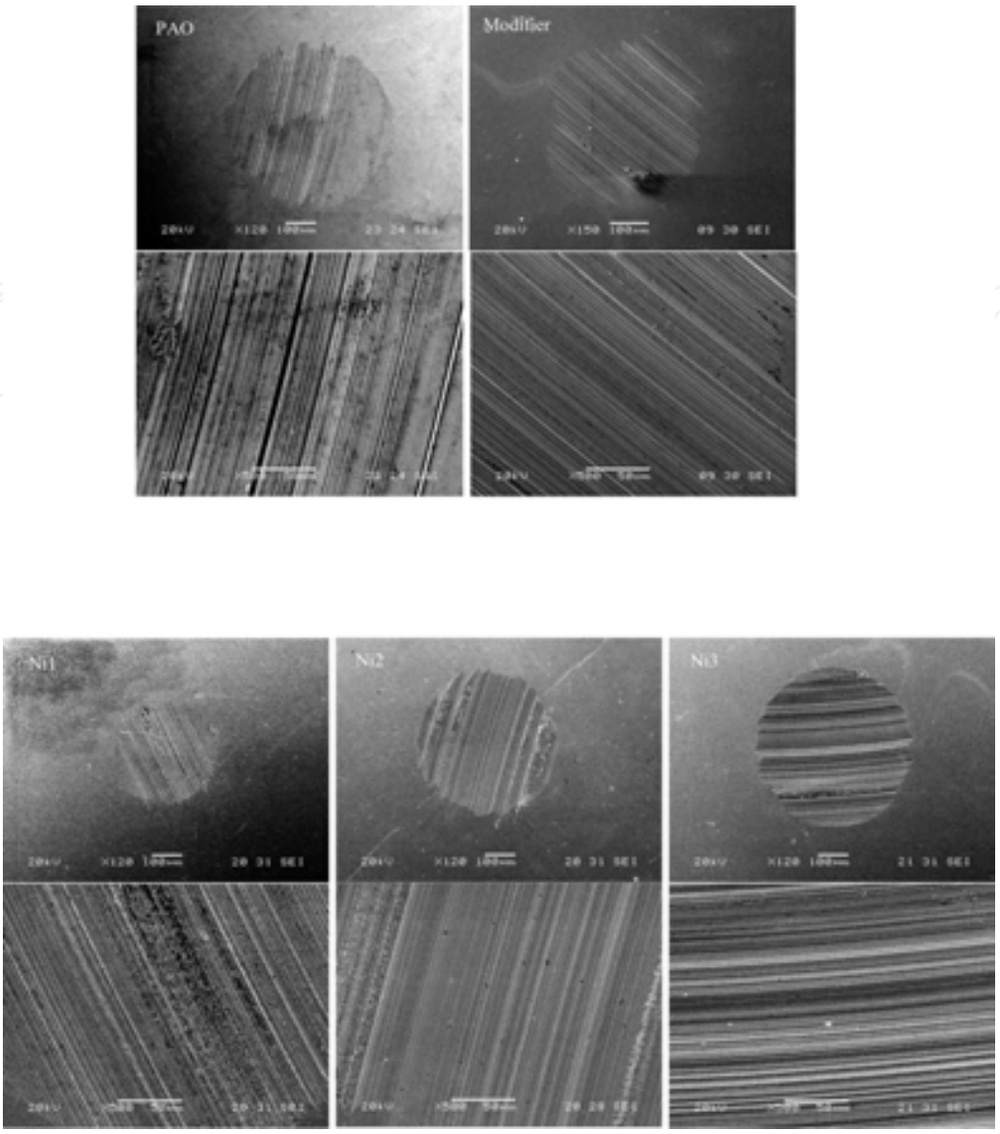

Figure 10. SEM micrographs of wear scars lubricated with PAO6 as well as PAO6 + surface-modifiers and nanolubricants containing 0.05% Ni nanoparticles (300 N, 30 minutes).

In order to reveal the friction-reducing and antiwear mechanism of Ni nanoparticles, chemical states of several typical elements on the worn surfaces of steel balls was analyzed by XPS. The XPS spectra of C 1s, O 1s, N 1s, Fe 2p, and Ni 2p on the worn surface of steel ball lubricated with PAO + 0.1% Ni1 nanoparticles are shown in **Figure 11**. Atomic concentrations of elements on worn surface are listed in **Table 2**. The C—N, COO—, C═C, —CH_2—, and —CH3 signals are attributed to chemically adsorbed and/or reacted surface modifier on sliding surfaces. The Fe 2p3/2 peaks at 710.90 and 713.16 eV are attributed to Fe_2O_3 [32]. It can be reasonably concluded that under selected experimental conditions ferrous oxides are formed on the worn surfaces of the steel balls. Moreover, Ni 2p3/2 peak at 852.58 eV and Ni 2p1/2 peak at 871.20 eV are attributed to Ni nanocores, which are released from surface-modified nanoparticles and transferred onto sliding surfaces during the rubbing process. Moreover, Ni 2p3/2 peak at 857.49 eV and Ni 2p1/2 peak at 876.20 eV (corresponding satellite peak is located at 862.40 eV and O

http://dx.doi.org/10.5772/64592

1s peak is located at 531.47 eV) indicated that a part of Ni nanocores can react with oxygen to form Ni_2O_3. In addition, as shown in **Table 2**, a higher atomic concentration of Ni, O, and N appeared on the worn surface lubricated by PAO6 + Ni1 than those lubricated by PAO6 + Ni2 and by PAO6 + Ni3, at the same time, the one lubricated by PAO6 + Ni3 has a higher atomic concentration of Fe. It can be deduced that nanolubricants with smaller size are able to form boundary lubricating film with good coverage on sliding surfaces thereby showing better antiwear ability.

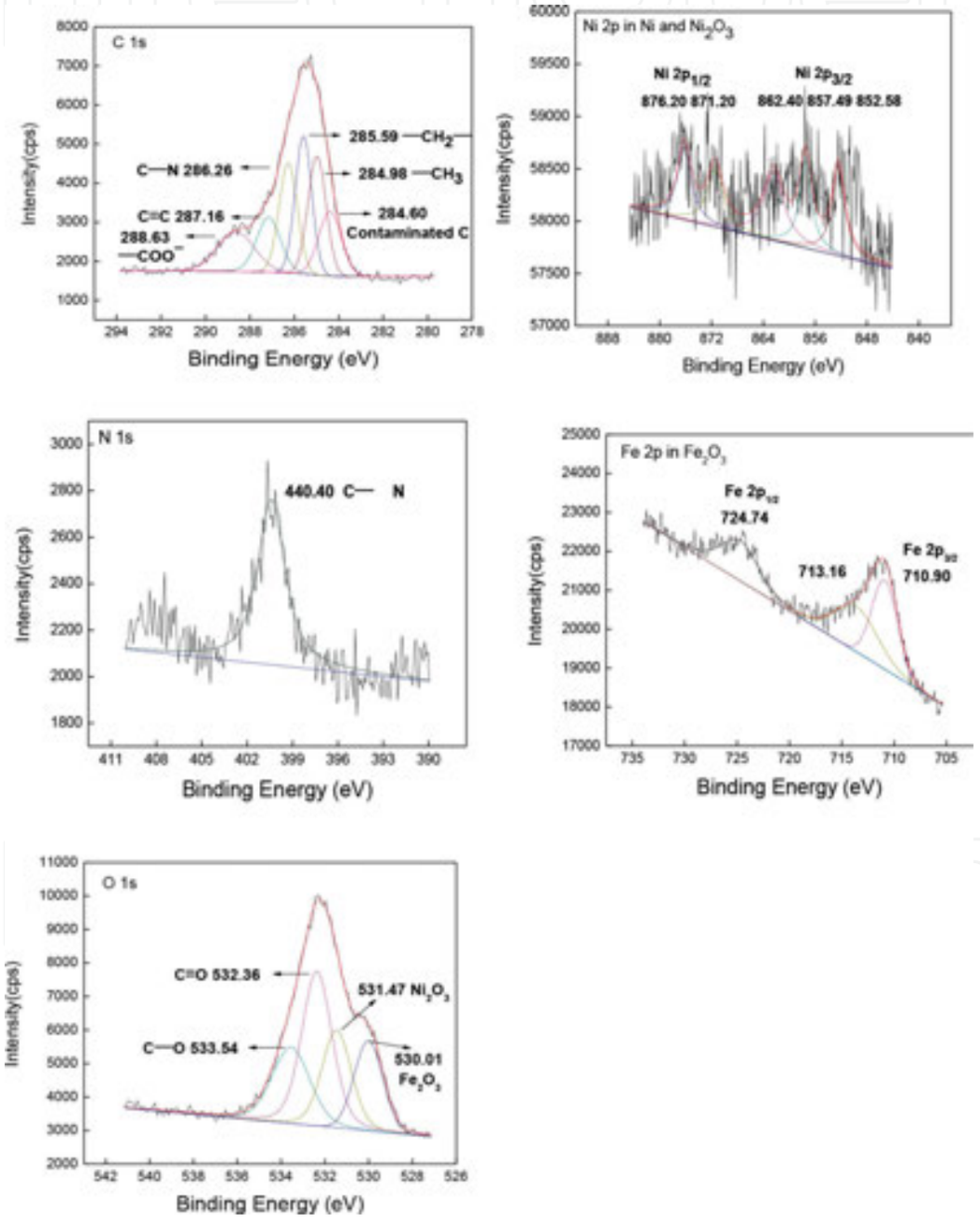

Figure 11. Curve-fitted XPS spectra of typical elements on rubbed surface of steel ball lubricated with nanolubricants containing 0.1% Ni1 (four-ball tribometer, 1450 rpm, 400 N, 30 minutes).

Based on the XPS results, it can be concluded that during sliding of the steel-on-steel contact nickel-based nanolubricants undergo tribochemical reaction and release organic surface modifier and highly chemically active Ni nanocores, which can be easily adsorbed on sliding surfaces and generate a boundary lubricating film thereby improving the antiwear ability [30]. Besides, smaller Ni nanoparticles are easier to fill up micropits and grooves on worn surfaces, and form a compact protective layer. As a result, the adsorbed and deposited Ni layer greatly contributes to improve the tribological properties of PAO6 base oil.

3. The effect of morphology Ni nanolubricant on its tribological properties

The properties of nanoparticle usually lie on the atom on surface, because the atomic bonds on the surface are unsaturated, and the chemical environment and electron cloud density of the surface atom is quite different from the atoms inside. The proportion and the type of atomic bonds of atom on the surface are decided not only by the size but also by the morphology of nanoparticles [33–36]. For example, Ag nanoparticle has a high catalytic activity, good electrical properties, and photocatalytic bactericidal activity, while flaky triangular Ag nanoparticles have great potential in biosensing and biomedical field. Ni nanoparticle with 15 nm diameter is superparamagnetic, while Ni nanoparticle with 85 nm diameter has high coercivity. The tribological mechanism of nanoparticle with different morphology should be better studied through one kind of nanoparticle. Surface modification can effectively improve the dispersion stability of nanoparticles in lubricating oil base [2–3], and surface modification can affect preferentially growing crystal plate. Nanoparticles with different shapes could be prepared through controlling conditions of surface modification. Ni nanoparticles with three different shapes were prepared through thermal decomposition of Ni $(HCOO)_2$ in decane modified with 12 alkyl sulfonate (DBS) and oleylamine (OAM).

Preparation conditions are listed in **Table 1**. Three morphologies of Ni nanoparticles were prepared by varying the concentration, molar ratio of reactants, and reaction time. XRD spectra of Ni nanoparticles with different shapes are shown in **Figure 12**. Three characteristic diffraction peaks: 44.5°, 51.8°, and 76.4° correspond to the crystal plate (111), (200), and (220) in face-centered cubic (FCC) structure of Ni (JCDPS No.7440-02). Diffraction peaks widening are significant for all samples. With the increase in modifiers content, widening phenomenon was much more obvious, which indicates that the Ni nanoparticle morphology, size, and crystallinity are affected in-depth by modifiers' contents.

Sample code	PAO volume (mL)	TEM diameter (nm)	Scherrer diameter (nm)
Ni1	80	7.5	6.0
Ni2	40	13.5	8.3
Ni3	20	28.5	10.0

Table 1. Size of as-prepared Ni nanoparticles determined by TEM observation and Scherrer equation.

http://dx.doi.org/10.5772/64592

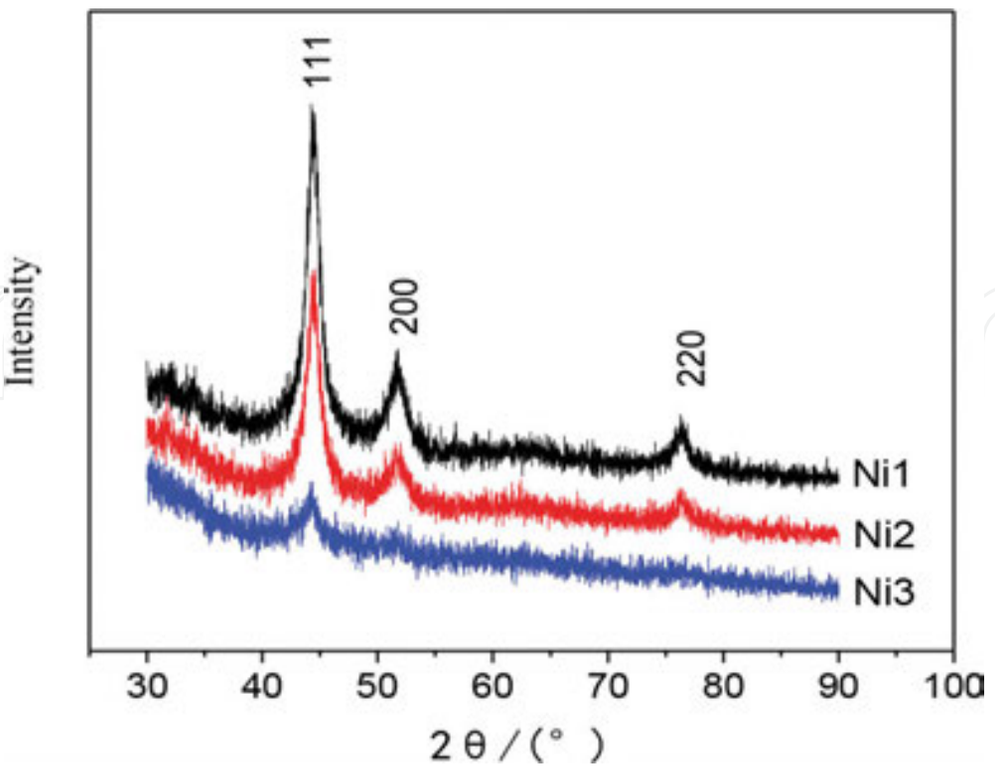

Figure 12. XRD patterns of Ni nanoparticles with different morphology.

The TEM images of Ni nanoparticles with different shapes are shown in **Figure 13** (low magnification on the left, high magnification on the right). Combined with the information of **Table 1**, it can be concluded that the shape of Ni nanoparticles is decided by the mol ratio of formic acid nickel to DBS. When the mol ratio is 5:1, the shape of Ni nanoparticles is spherical; when the mol ratio is 3:1, the shape is triangular plate; and when the ratio is 1:2, the shape of the Ni nanoparticles is triangular rod. Because of the inducement of surface modifier different crystal plate of Ni nanoparticles grows differently, which leads to different shapes. In addition, Ni nanoparticle shows narrow size distribution. No obvious aggregation appears because of the surface organic modification.

To further examine the interaction between the organic surface modifier and Ni nanocore, we conducted FTIR analysis of surface-modified Ni nanoparticles as well as pure OAM and OA. As shown in **Figure 14**, the characteristic absorption bands of pure OAM at 3367 and 3295 cm^{-1} correspond to the symmetric and asymmetric stretching vibration of N-H, and the absorption bands at 1583 and 967 cm^{-1} belong to the shear and flexural vibration mode of $-NH_2$ [27]. For a solid DBS, absorption peaks at 1183 and 1053 cm^{-1} correspond to asymmetric and symmetric stretching vibration of S=O. In addition, for pure OAM and DBS, characteristic peak of nonpolar chain appears, which is stretching vibration peak of CH_3 and CH_2 at 2922 and 2852 cm^{-1}, C—H bending vibration peak at 1464 cm^{-1}, and not less than four consecutive methylene rocking vibration peak at 720 cm^{-1} [28]. For surface modified Ni nanoparticles, the existence of nonpolar chain in surface modifiers OAM and DBS can be confirmed by characteristic peaks at 2922, 2852, 1464, and 720 cm^{-1}. For surface

modified Ni nanoparticles, the primary amino characteristic peaks at 3367, 3295, 1583, and 967 cm^{-1} do not appear; however, the stretching vibrations peak of c═c at 1629 cm^{-1} and asymmetric and symmetric stretching vibrational peaks of S═O at 1183 and 1053 cm^{-1} appears. Therefore, it can be concluded that surface modifiers (OAM and DBS) and Ni nanoparticles are chemically combined, and this stable chemical bond effectively blocks reunification and oxide particles of Ni; meanwhile, nonpolar chain improves its compatibility with base oil.

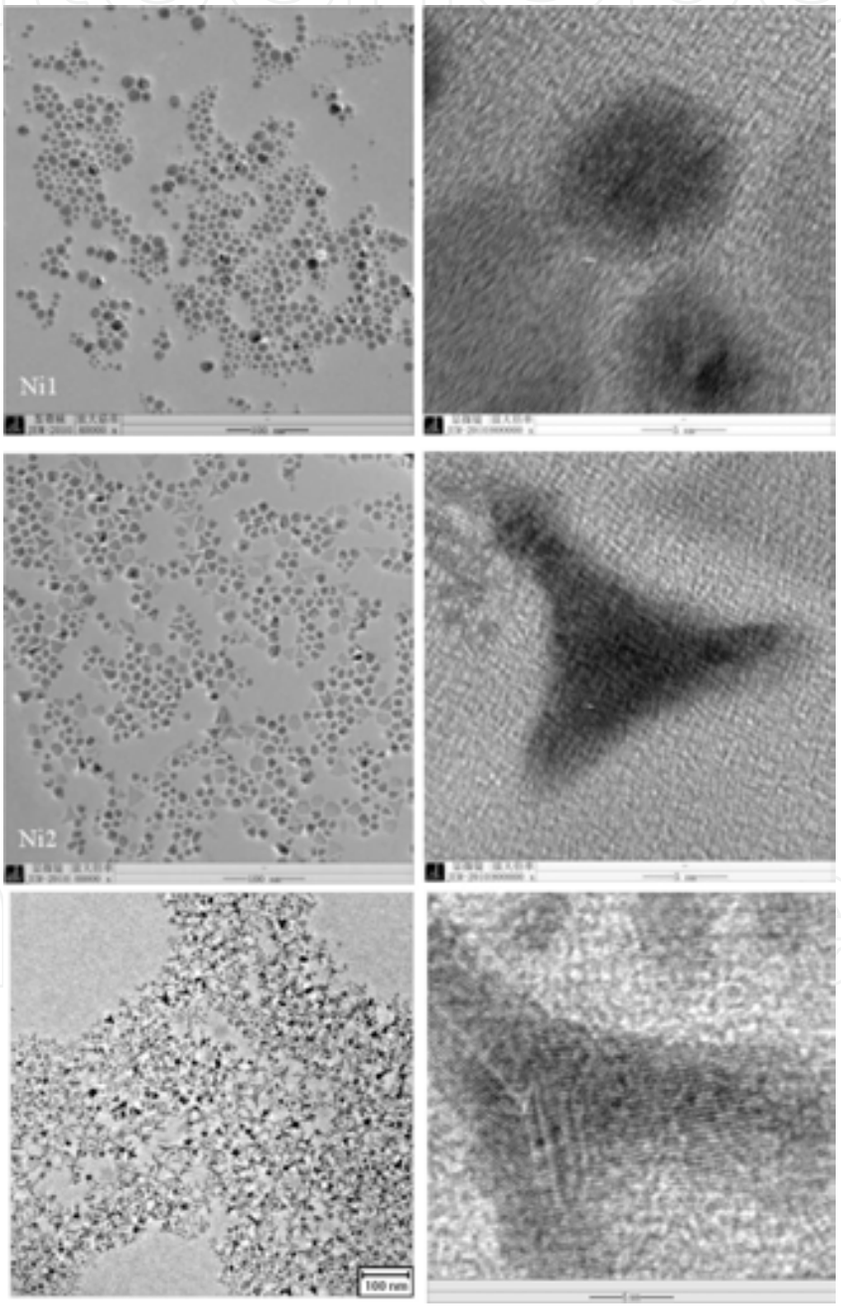

Figure 13. TEM (left) and enlarged (right) images of Ni nanoparticles with different morphology.

http://dx.doi.org/10.5772/64592

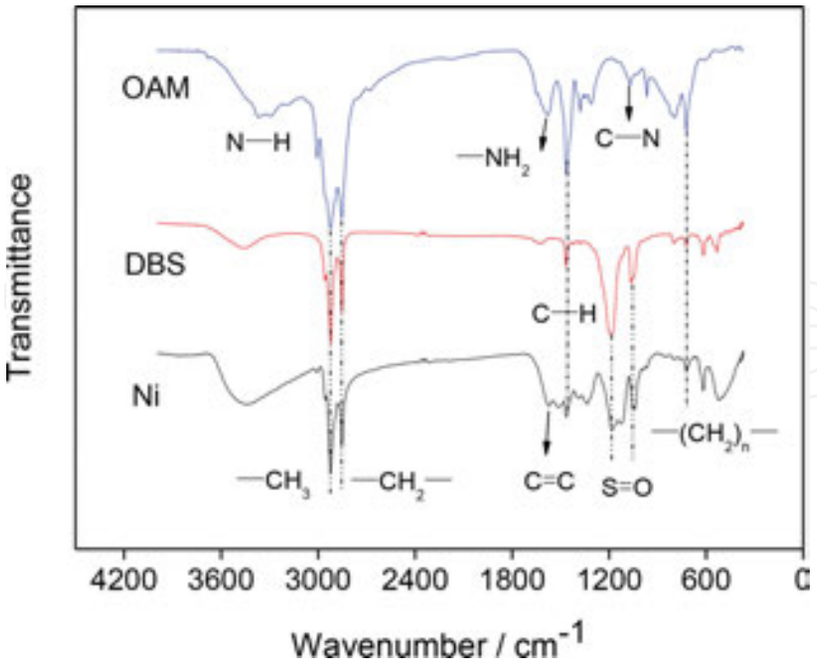

Figure 14. FTIR spectra of DBS, OAM, and as-separated Ni nanoparticles.

The variation of friction coefficient and wear scar diameter with the concentration of Ni is shown in **Figure 15** (four ball machine, 300 N, 1450 rpm, 30 minutes). It can be seen that the friction reduction and antiwear properties of Ni nanoparticles is closely related with its shape and concentration. Compared with the base oil PAO, within a suitable concentration range, Ni1 and Ni3 nanoparticles present a certain friction reduction property, while Ni2 nanoparticles significantly improve the wear resistance of PAO. In the experiment concentration range, Ni2 (triangular plate) is more effective than Ni1 (spherical shape) and Ni3 (triangular rode) in reducing WSD of steel partner. Therefore, it can be deduced that Ni nanoparticles with triangular plate shape easily forms a continuous film on the sliding surface, which prevents direct contact between friction interface so as to prevent the adhesion, thus showing a better abrasion resistance.

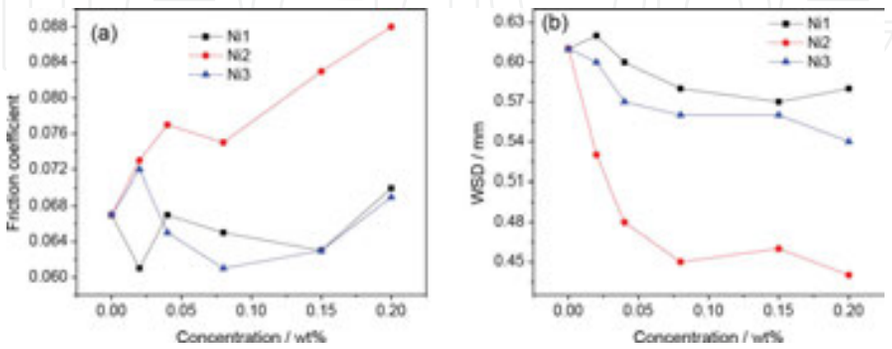

Figure 15. Variation of friction coefficient (a) and wear scar diameter (b) with the concentration of Ni nanoparticles (four-ball friction and wear tester, 1450 rpm, 300 N, 30 minutes).

Figure 16 showed variation of coefficient under (a) and the wear scar diameter (b) with the load (four-ball, 1450 rpm, 30 minutes). For pure PAO6 and PAO6 added with 0.2% Ni nanoparticles, the coefficient of friction decreases with the increasing of load. Under higher load, addition of Ni nanoparticles can reduce friction, while for the whole test load, three shapes of Ni nanoparticles can effectively improve antiwear properties of PAO6 base oil. Especially for triangular plate-like Ni2, the WSD can be reduced by 35%. It may be due to its easy adsorption on steel sliding surface and formation of lubricating film, which leads to better antiwear capacity.

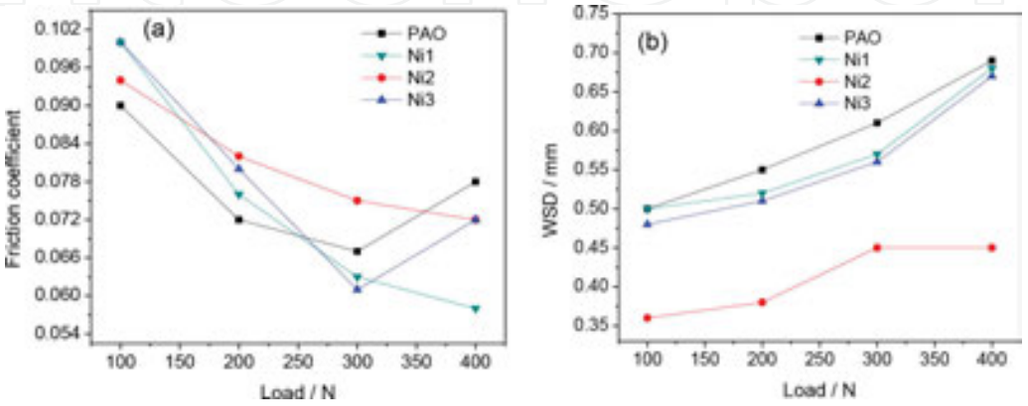

Figure 16. Friction coefficient (a) and wear scar diameter (b) versus applied load under the lubrication of PAO6 and 0.2% Ni nanoparticles with different morphology (four-ball friction and wear tester, 1450 rpm, 30 minutes).

Figure 17 shows the P_B and P_D of PAO6 and Ni nanoparticles of three morphologies. As shown in the figure, P_D values show no difference, but addition of Ni nanoparticles can improve extreme pressure properties of PAO6, especially for triangular plate Ni, its EP is the best. This suggests that surface modified Ni nanoparticles can effectively improve the bearing capacity of PAO6.

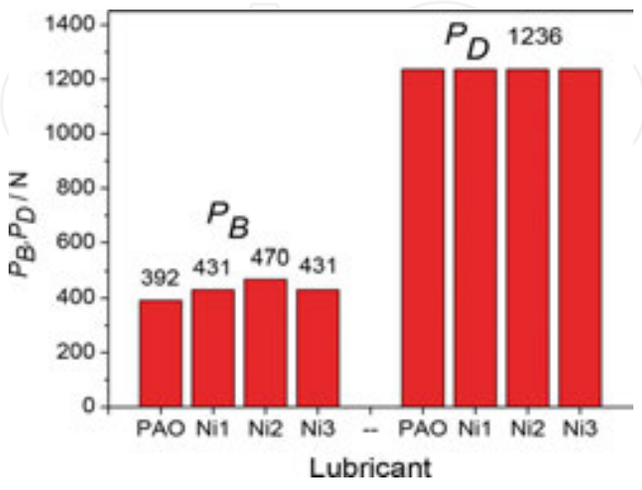

Figure 17. $P_B$and $P_D$values of various lubricant systems (four-ball friction and wear tester, 1450 rpm, 10 seconds).

http://dx.doi.org/10.5772/64592

SEM micrographs of wear scars lubricated with PAO6 as well as PAO6 containing 0.2% Ni nanoparticles are shown in **Figure 18**. Deep plow ditch and marks of tearing between friction pairs appears on the worn surface lubricated with PAO6. Lubricating effect of different Ni nanoparticles is obviously different. Compared with Ni1 and Ni3, WSD of steel ball lubricated with Ni2 is the least, and the worn surface is the smoothest. For the nanoparticle Ni1 and N3, there is some designated marks and stick. Once again, it is proved that triangular plate Ni nanoparticles have better abrasion resistance.

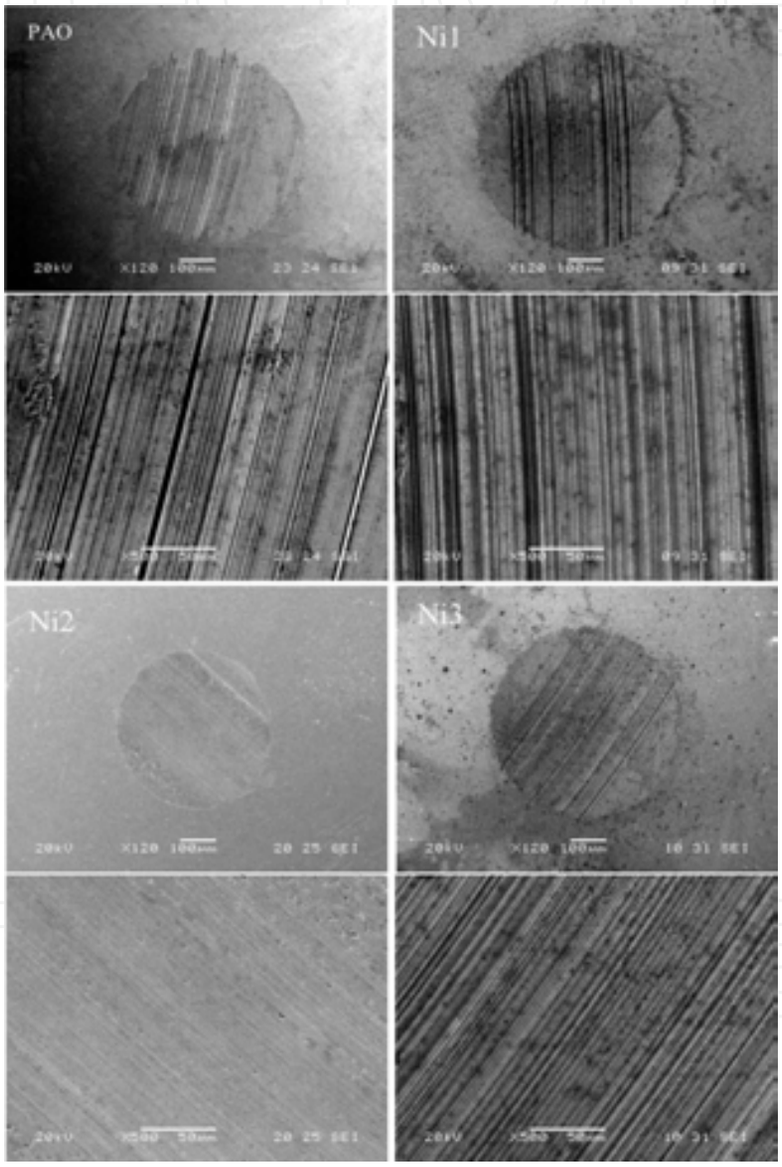

Figure 18. SEM micrographs of wear scars lubricated with PAO6 as well as PAO6 containing 0.2% Ni nanoparticles (four-ball friction and wear tester, 1450 rpm, 300 N, 30 minutes).

The worn surfaces of the steel balls lubricated with different lubricant are analyzed by mean of XPS so as to acquire more information about the tribochemical reactions involved during the friction process. **Figure 19** shows the curve-fitted XPS spectra of C1s, N1s, O1s, S2p, Fe2p,

and Ni2p on the worn surface of steel ball lubricated with nanolubricants containing 0.2% Ni (four-ball, 1450 rpm, 400 N, 30 minutes). It can be noticed that S, O, N, and C are detected on the worn surface. This indicates that surface modifier DBS and OAM are adsorbed on the worn surface or takes part in the tribochemical reaction during the sliding process.

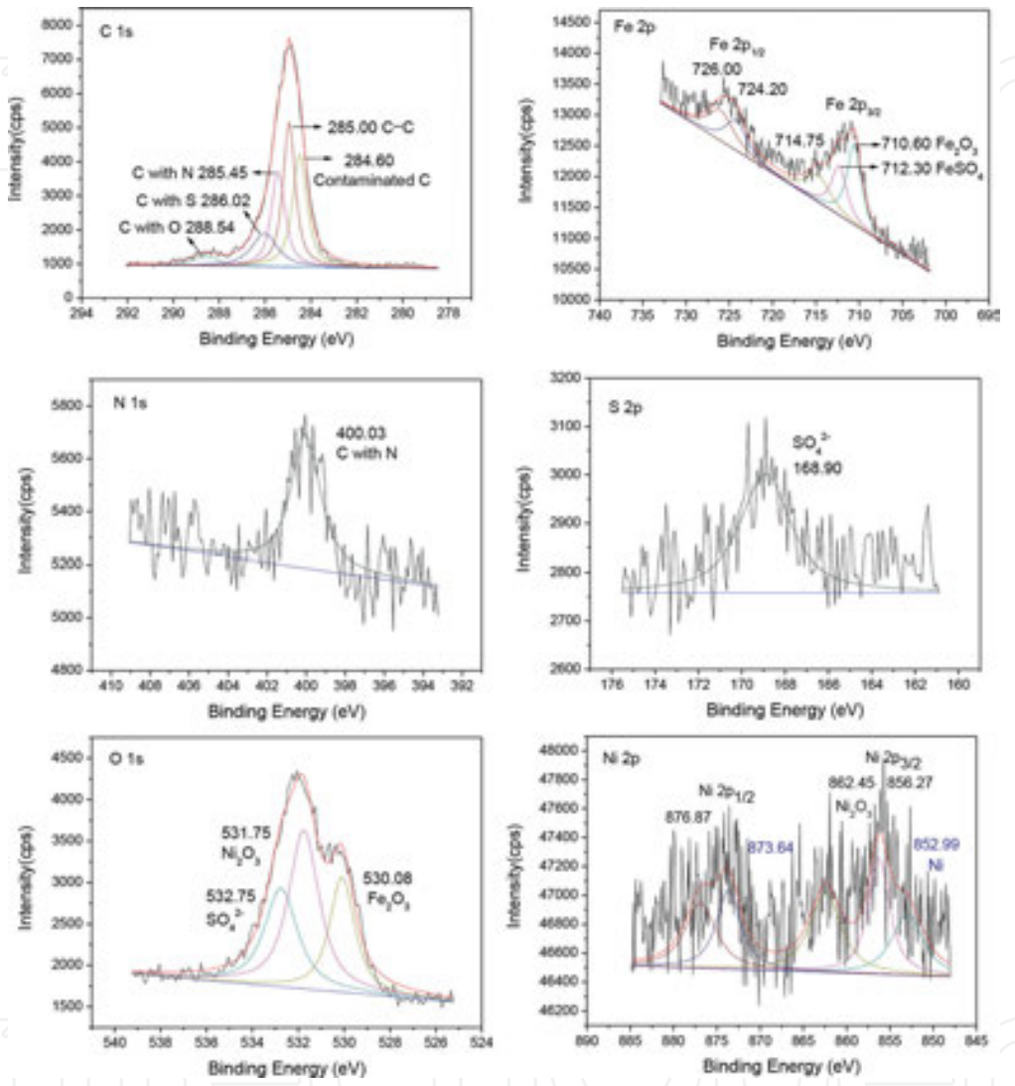

Figure 19. Curve-fitted XPS spectra of typical elements on rubbed surface of steel ball lubricated with nanolubricants containing 0.2% Ni (four-ball friction and wear tester, 1450 rpm, 400 N, 30 minutes).

It can be seen that the Fe2p shows XPS peaks at the binding energies 710.60, 712.30, 724.2, and 726.00 eV. The peak at a binding energy of 710.60 and 724.20 eV corresponds to the Fe_2O_3 [32]. The peak at 712.30 and 726.00 eV corresponds to the $FeSO_4$. This indicates that ferrous oxides have been formed on the worn surface, and the surface modifier DBS reacted with steel ball during the sliding process.

Ni 2p shows XPS peaks at the binding energies 852.99 and 856.27 eV. The peak at a binding energy of 852.99 eV corresponds to the Ni 2p3/2, and the peak at 856.27 eV corresponds to

Ni_2O_3. This indicates that Ni nanoparticles transferred to the worn surface of steel ball, and part of it was oxidized.

When the element O is mentioned, the binding energy of O1s is about 530.08, 531.75, and 532.75 eV. The binding energy at 530.08 eV corresponds to the Fe_2O_3 while the peak at 531.75 eV corresponds to the Ni_2O_3. The binding energy at 532.75 eV corresponds to the sulfate radical.

Based on the analysis of XPS, it can be inferred reasonably that, during the process of sliding between steel and steel, under low load, the organic surface modifiers outside the Ni nanoparticles could easily be adsorbed to the surfaces of friction pairs generating the layer of organic lubricating film. Under high load, the friction generated by mechanical, chemical, and electrochemical action of friction, and nano-Ni exchange of energy and material exchange between, to form a metal on the friction surface protective film, metal oxide protective film for metal sulfate, separated from the friction surface, play as antiwear and friction. For, the lubricating effect of Ni nanoparticles with different shapes, the Ni nanoparticle with shape of triangular sheet shows the best lubricating effect, which could be attributed to its larger contact area with sliding surface and, more easily absorbing on the worn surface and forming boundary lubricating film.

4. Tribological properties of Ni nanolubricant in DIOS/DLC solid-liquid composite lubricating system

Diamond-like carbon (DLC) coatings are becoming attractive protective films for many automotive parts as they offer high hardness, ultralow friction, and good wear resistance under dry or lubricated contacts [37–42]. However, the key problem with their lubrication is a low reactivity toward existing additives and oils [43, 44]. Although it was confirmed that DLC coatings react with these metal-tailored additives, their interactions are much weaker and the formation of tribochemical films was much lower and difficult to control. On the other hand, today's most effective additives will need to be reduced or phased out in the near future for environmental reasons and replaced with greener lubrication technologies.

Kalin' research group reported the lubrication behaviors of MoS_2 nanotubes as a green, physically based additive for DLC-based solid-liquid synergetic system [45]. The addition of MoS_2 nanotubes (with diameters of 100 nm and length of 20 μm) to PAO oil significantly improved the friction behavior in the boundary- and mixed-lubrication regimes. However, for the elasto-hydrodynamic lubrication (EHL) regime, the effectiveness disappeared completely. The study results of EHL suggested that the classical EHL modes are accurate down to films, as thin as 10–20 nm [46]. Hamed Ghaednia and Hasan Babaei reported the friction reduction of nanoparticle (with diameter of 7 nm) in EHL regime, and proposed that the obstructed flow induced by nanoparticles of friction reduction mechanism reduced the friction between layers of lubrication molecules. So, nanoparticle additives with size bigger than the oil film thickness would prevent the occurrence of EHL. The research about nanoparticles additives for DLC-based, solid-liquid synergetic system is considered rare. Moreover, the study about the

lubrication of solid-liquid synergetic system constructed from DLC coatings and real nanofluid (nanoparticle with diameter of less than 10 nm) has not been reported.

We show in this study that the Ni nanoparticle (7 nm in diameter) significantly reduces the friction in the DLC/steel contacts lubricated by fully formulated oil di-iso-octyl sebacate (DIOS) in all lubrication regimes: boundary, mixed, and elasto-hydrodynamic lubrication. Analysis of the composite and topography of worn surface was operated systematically in order to reveal the friction reduction mechanism.

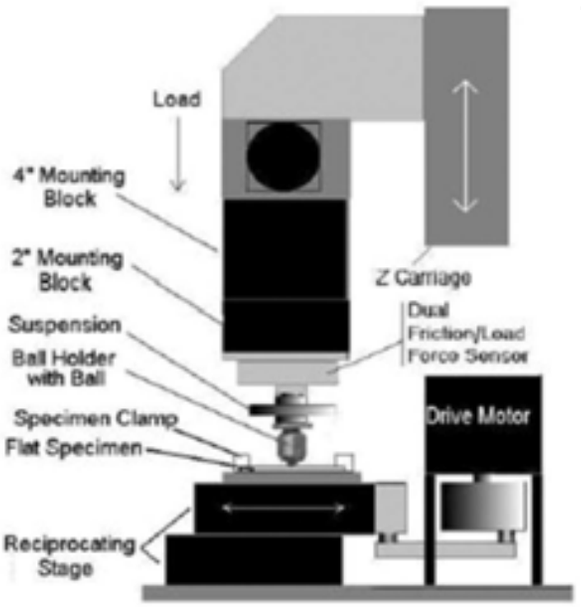

Figure 20. Schematic diagram of UMT tribometer.

The tribological properties of DLC and DLC/DIOS solid-liquid composite system were measured on a ball-on-disk tribometer shown in **Figure 20**. GCr 15 steel ball was used as friction pair with a diameter of 4 mm. Its elastic modular and Poisson ratio was 205 GPa and 0.28, respectively. In order to study the lubricating mechanism of Ni nanoadditive in DLC/DIOS solid-liquid system, three lubricating conditions were used including dry friction with DLC, solid-liquid composite lubricating by DLC/DIOS, and DLC/DIOS added with Ni nanoparticles. All of the friction tests were performed through a reciprocating sliding test mode at ambient temperature with a load range from 0.5 to 4 N. The relative humidity was 20–40%. Each test was repeated three times with a stroke of 5 mm. In order to obtain the Stribeck curves, a wide range of average contact velocities from 60 to 480 rpm were applied to achieve different lubrication regimes, i.e., boundary, mixed, and elastro-hydrodynamic. Because of the characteristics of reciprocating motion, within the stroke some variation in regimes may occur as a consequence of varied velocity. However, this has negligible effect in boundary and mixed lubrication. In elastro-hydrodynamic lubrication (EHL) regime, it is clear that EHL cannot be achieved at end-stroke. Accordingly, in this work for the region claimed as the EHL regime, these conditions are fully valid only within the central part of the stroke. Moreover, in the

http://dx.doi.org/10.5772/64592

central part of the stroke where velocity is higher than the average, the conditions are even more beneficial toward EHL than "average" calculations for the lambda parameter.

The coefficient of friction under the three lubricating conditions is shown in **Figure 21** (4 N load and sliding speed 240 rpm). It can be seen that with the increasing of friction time, the coefficient of friction lubricated by DLC and DLC/DIOS fluctuated slightly, while that of DLC/DIOS added with Ni nanolubricant is very stable. The coefficient of friction decreased greatly under DLC/DIOS and DLC/DIOS added with Ni nanolubricant lubricated conditions, and DLC/DIOS with Ni nanolubricant composite lubrication system shows better antifriction effect.

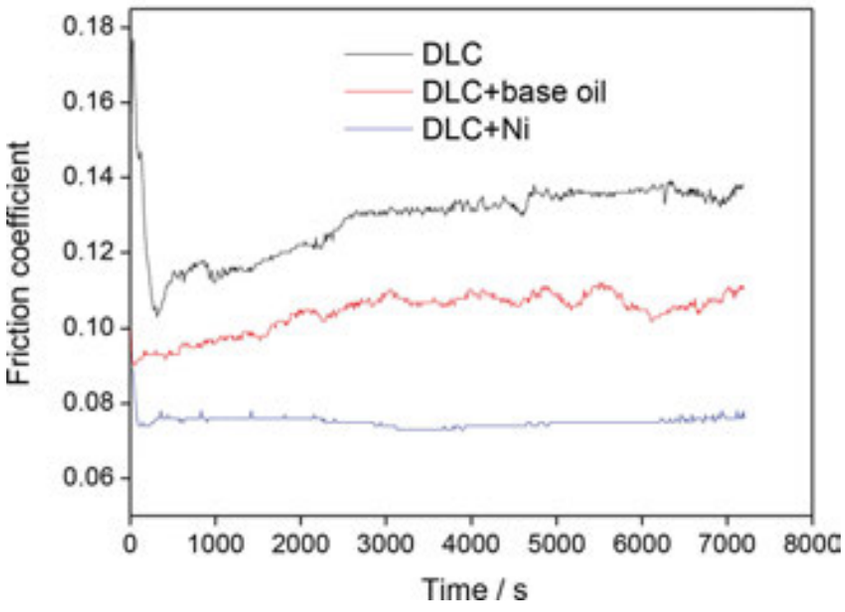

Figure 21. Coefficient of friction versus time under three lubricating conditions.

The effect of sliding speed on coefficient of friction under the three lubricating conditions is shown in **Figure 22**. As can be seen, coefficient of friction lubricated by DLC/DIOS and that added with Ni nanolubricant decreases rapidly with the sliding speed, while that of dry friction with DLC film is almost unchanged. With the increasing of sliding speed, lubricating regime changes from boundary lubrication to mixed lubrication. DLC/DIOS solid-liquid composite lubricating system and that added with Ni nanolubricant greatly reduces the coefficient of friction of the DLC film, and at low speed the antifriction effect of DLC/DIOS with Ni nanolubricant is more outstanding.

Based on the graphite transfer film theory of DLC, the metastable carbon DLC films overcome energy barrier during the friction process and transform into graphite structure [47–49]. In graphite structure, the weak interlayer binding force between layers leads to lower shear strength that reduces the coefficient of friction, which results in good antifriction effect of DLC films. The Ni nanolubricant added in DLC/DIOS lubricating system could absorb on the sliding

surface and form a lower shear strength film, and then reduce the friction between friction surfaces.

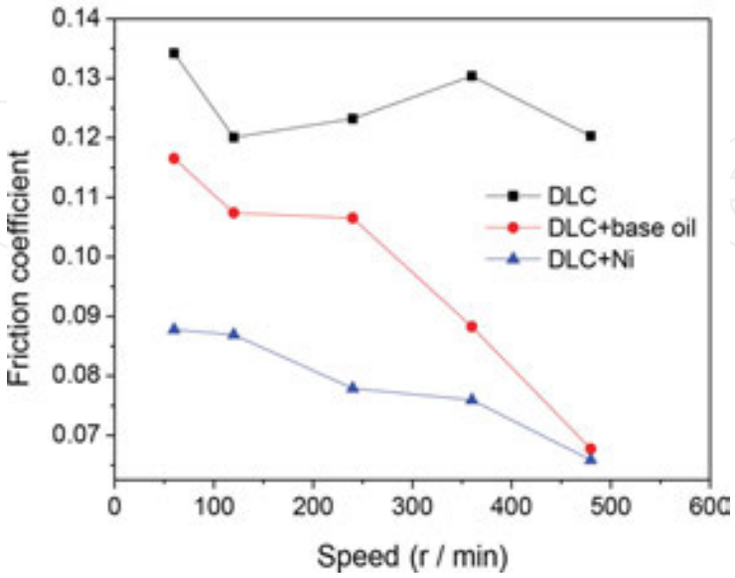

Figure 22. Coefficient of friction versus sliding speed under three lubricating conditions.

The effect of load on coefficient of friction under the three lubricating conditions is shown in **Figure 23**. With the increase of load, the coefficient of friction under dry friction and Ni nanolubricant lubricating conditions were slowly declining, and for those lubricated with DLC/DIOS, the COF fluctuated. The effect of load on the friction coefficient is less, but the existence of base oil lubrication and Ni nanolubricant greatly reduces the friction coefficient of DLC films, and the Ni nanolubricant makes the coefficient of friction more stable.

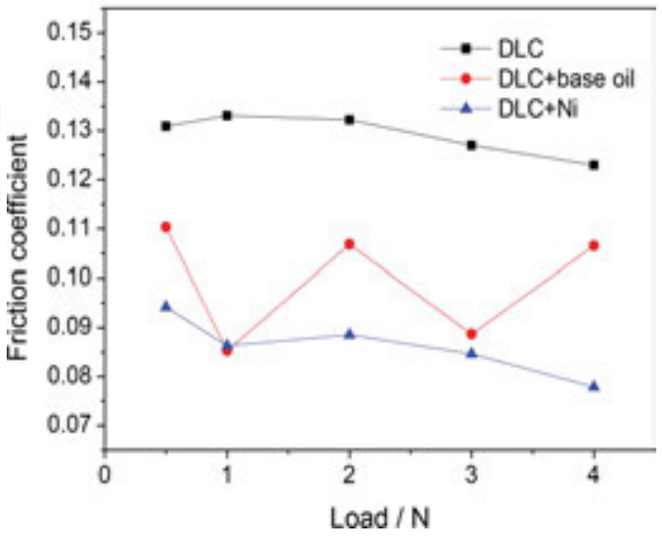

Figure 23. COF versus load under three lubricating conditions.

http://dx.doi.org/10.5772/64592

The wear rate of DLC films under the three lubricating conditions is shown in **Figure 24** (4 N load, sliding speed of 240 rpm time was 4 h). Under the experimental conditions, the wear rate of DLC decreases by 72% and 86%, respectively, because of lubricating of DIOS and Ni nanolubricant. Thus, antiwear effect of Ni nanolubricant composite lubricating is better.

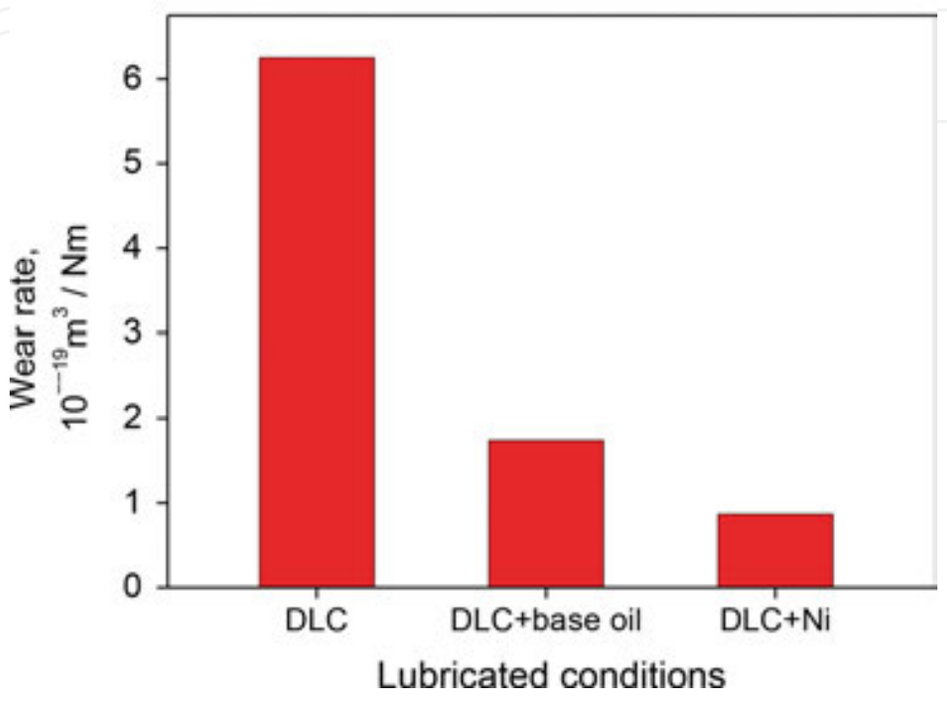

Figure 24. Wear rate of DLC films under three lubricating conditions.

The SEM images of wear scar on DLC films under the three lubrication conditions is shown in **Figure 25** (4 N load, sliding speed of 240 rpm, 4 h). As can be seen, under dry friction, the wear mark of DLC film is widest with grooved surface strip, and obviously has certain adhesive wear; while under the lubricating of DLC/DIOS, the wear mark is significantly smaller and shallow. For the DLC/DIOS with Ni nanolubricant, the wear mark is the most narrow (<100 m) and the surface is very smooth. Therefore, Ni nanolubricant greatly increases the antiwear effect of composite lubricating system, which is consistent with the above analysis of wear rate.

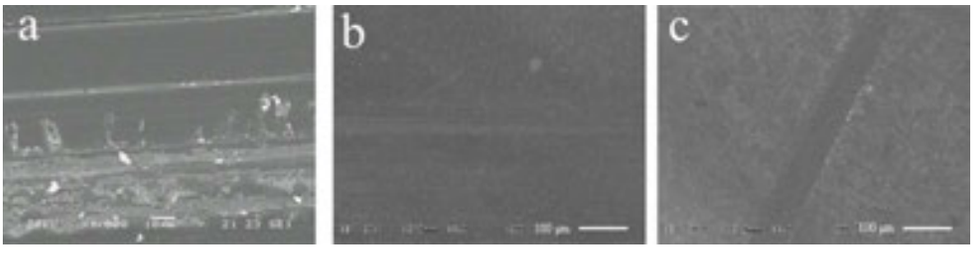

Figure 25. SEM images of wear scar on DLC films under three lubrication conditions.

For comparison, the SEM images of wear scar on steel balls under the three lubrication conditions are also shown in **Figure 26**. The wear scars under different conditions are quite different. Under dry friction the wear scar is the largest, with obvious edge debris in which the black substance may be graphitized transfer film. For DLC/DIOS and that added with Ni nanolubricant, wear scars are obviously smaller with less debris on their edges, the worn edge grinding on grinding ball mill is less. There are some shallow scratch grooves on the steel ball under DLC/DIOS lubrication condition; for that with Ni nanolubricant, the wear scar surface is smooth without any grooves and debris. Therefore, it can be concluded that DLC/DIOS with Ni nanolubricant composite lubricating system shows good synergistic effect of antiwear and antifriction, which is consistent with the above analysis.

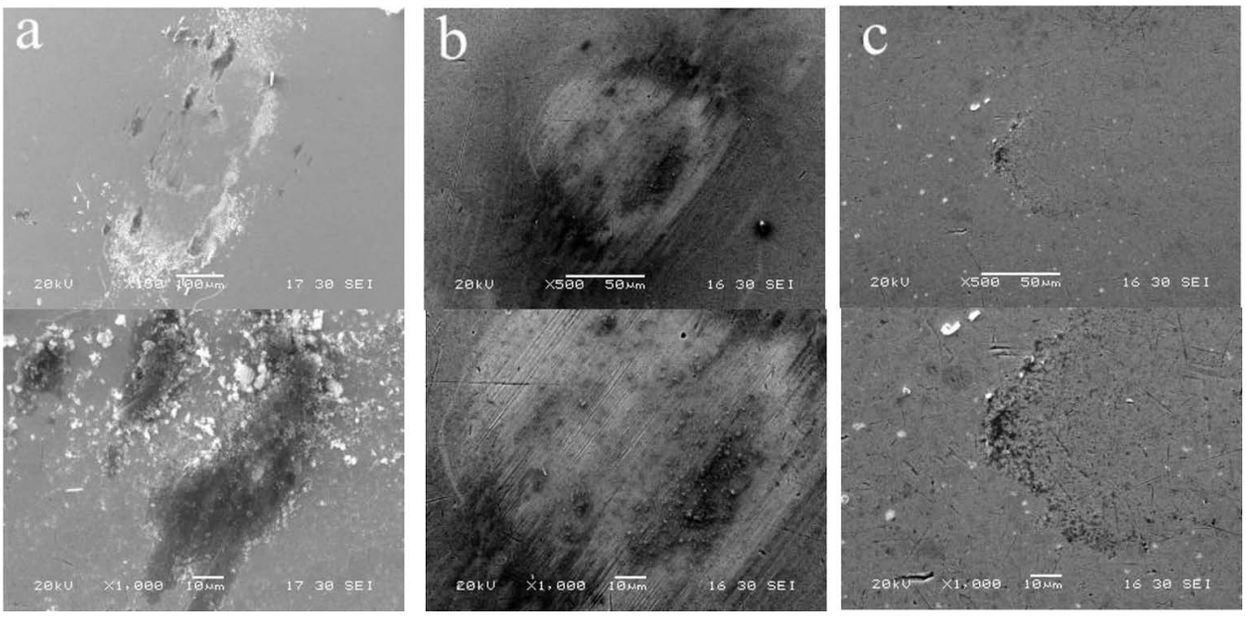

Figure 26. SEM images of wear scar on steel balls under three lubrication conditions.

The Stribeck curve describes the variation of friction coefficient with the contact conditions and shows lubricating regimes conversion between elasto-hydrodynamic lubrication, mixed lubrication, and boundary lubrication, which is a simple and effective method for judging lubricating regimes and predicting coefficient of friction [50–55]. Through comparing coefficient of friction under different lubrication regime, for example, the difficulty into EHL lubrication regime and the bottom width of it, the lubricating performance of lubricant can be valued comprehensively. Therefore, Stribeck curve was measured under lubrication of DLC/DIOS and that with Ni lubricant, which is shown in **Figure 27** (Sommerfield parameters was calculated according to [54]). In all lubrication regimes, the coefficient of friction of Ni nanolubricant is far better than that of base oil. Compared with lubrication condition of DLC/DIOS, the mixed lubrication regime is more stable and wider under lubrication condition of Ni nanolubricant, which can be attributed to the high chemical activity of Ni nanolubricant forming a solid adsorption film easily on the friction surface, so as to reduce friction resistance and exhibiting excellent tribological properties in the boundary and mixed lubrication regimes.

http://dx.doi.org/10.5772/64592

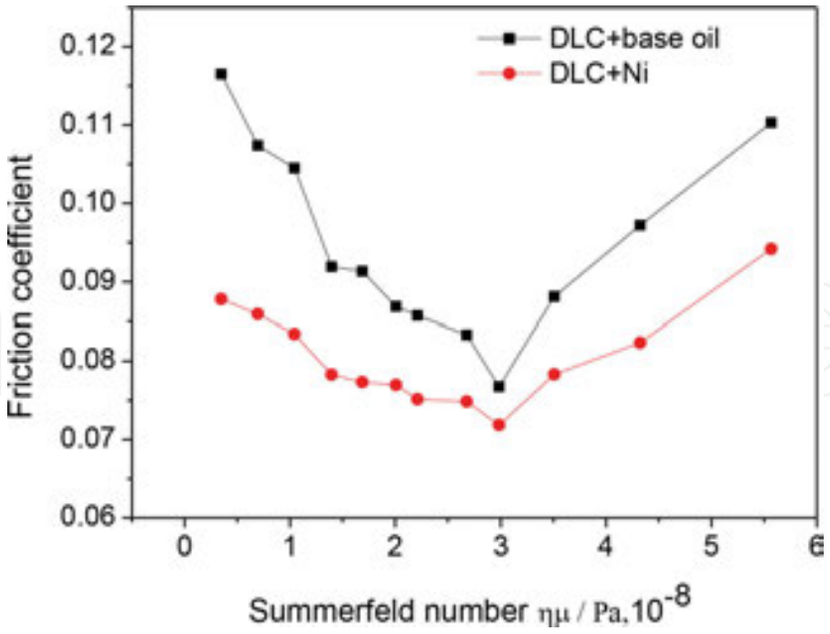

Figure 27. Stribeck curves of solid-liquid composite lubricating systems.

5. Tribological properties of Cu@Ni nanolubricants

In recent years, Cu nanoparticles as metal nanoadditives shows good antiwear and dynamic self-repairing performance [2–5, 7–10, 33–36]. For example, in this group, two alkyl two phosphorothioate (DDP) surface-modified Cu nanoparticles with average diameter of 5 nm was produced through *in situ* surface modification and liquid phase chemical reduction technology. As lubricating additives this Cu nanoparticles exhibit excellent energy saving, lubrication, antiwear, and self-repairing performance [34], which have been achieved in industrial production, and achieved considerable economic benefits. However, the modifier contains S, P elements, which easily leads to catalyst poisoning and environmental hazard, so is restricted for use in application process only.

If modifier does not contain S, P elements, Cu nanoparticles are easily oxidized [56–59]. How to produce stable Cu nanoparticles without S, P elements? Preliminary work shows that Ni nanoparticles are relatively stable and shows good antiwear performance. Then synthesis of Cu@Ni nanoparticles is going to be an effective method. Ni as shell can increase the stability of the center particles of Cu, which will further improve the tribological properties of nanoparticles [60, 61].

In situ preparation synthesis process of Cu@Ni nanoparticle is shown in **Figure 28**. Based on the difference of decomposition temperature of Cu $(HCOO)_2$ and Ni $(HCOO)_2$, the two compounds decomposes successively in basic oil of PAO6, Cu (HCOO) 2 decomposes first and forms Cu nucleus. Ni $(HCOO)_2$ decomposes subsequently. Because of the lower nucleation energy for heterogeneous nucleation, Ni forms nucleus on the surface of Cu nanoparticles and then forms

Ni coating on it. Therefore, a simple one-step synthesis method is set up for preparing Cu@Ni nanolubricant in basic oil, which is crucial for the application of nanolubricant.

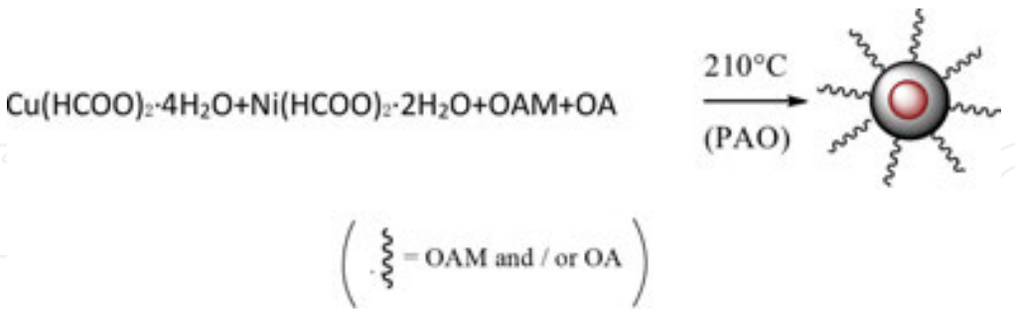

Figure 28. Synthetic procedure for preparing Cu@Ni nanoparticles.

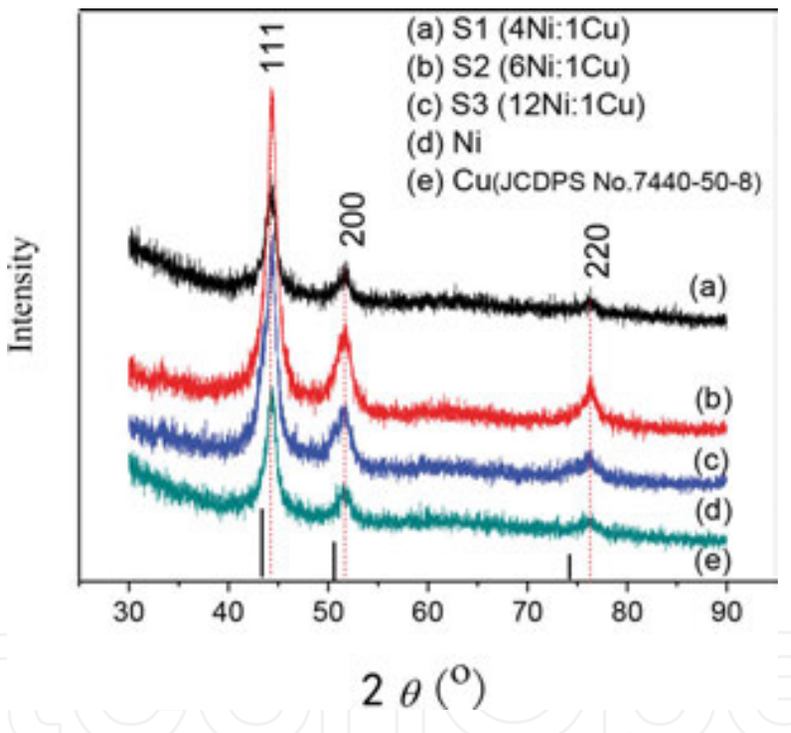

Figure 29. XRD patterns of Cu@Ni nanoparticles with different Cu content.

XRD maps of Cu@Ni nanoparticles with different Cu content are shown in **Figure 29**. For comparison, XRD map of pure Ni nanoparticles under the same conditions is also shown. It can be seen that three peaks at 44.5, 51.8, and 76.4 degrees corresponds to the (111), (200), and (220) crystal face of face-centered cubic (FCC) Ni (JCDPS No. 7440-02), respectively. There are no obvious characteristic peaks of Cu (JCDPS No. 7440-02). It may be that the grain size of Cu nucleus in Cu@Ni nanoparticles is too small (as shown in **Table 2**), and the XRD peak of Cu nucleus is remarkably broadened. In order to prove the existence of Cu nucleus, XPS analysis is used, which is shown in **Figure 30**. Cu@Ni nanoparticles Cu, Ni XPS, the binding energy at

peaks of 932.85 and 952.67 eV corresponds to Cu 2p1/2 and Cu 2p3/2, signs of oxidized Cu do not appear. So the stability of nano-Cu can be improved.

Sample code	Ni:Cu	Solution A (mL)	Scherrer diameter (nm)
S1	4:1 (12:3)	1.5	8.4
S2	6:1 (12:2)	1.0	7.3
S3	12:1	0.5	6.2

Table 2. Size of as-prepared Cu@Ni nanoparticles determined by Scherrer equation.

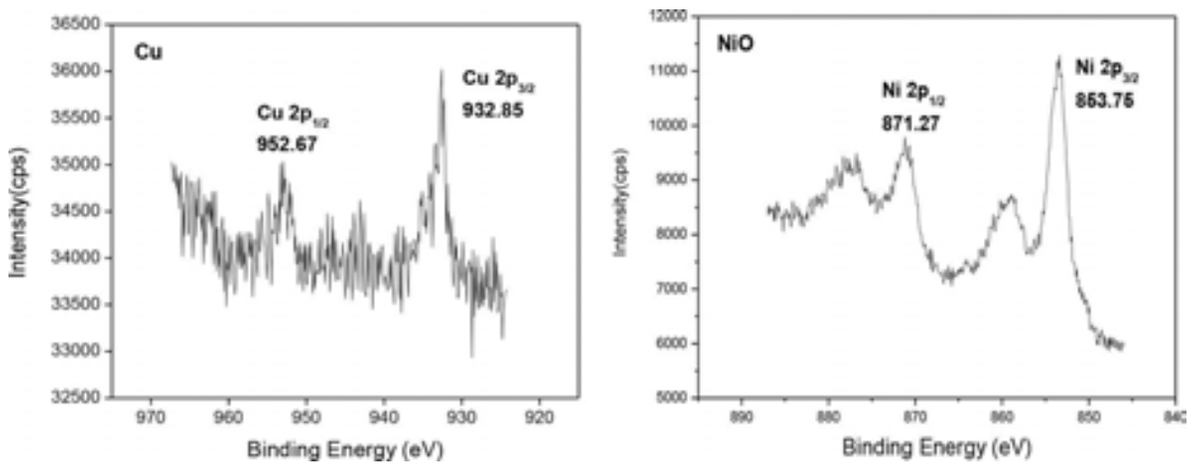

Figure 30. XPS spectra of Cu 2p, Ni 2p in Cu@Ni nanoparticles.

TEM images of Cu@Ni nanoparticles containing different amounts of Cu are shown in **Figure 31** (the panorama is on the left, the partial enlarged detail is on the right). It can be seen that Cu@Ni nanoparticles are uniform, spherical particles without obvious agglomeration, the average diameter is 12~15 nm. The coating outside of samples S1 and S2 is obvious, in which slightly shallow shell is Ni coating, the black core is Cu; for S3, Cu content may be too little to see. At the same time, binary modifier and controlling relative content of OAM and OA is crucial for synthesis, in which OAM is used as reducing agent controlling nanocrystal nucleation rate, high effect modifier of OA block the growth of nanocrystals, and the synergistic reaction of OAM and OA results in the monodispersed Cu@Ni nanoparticles.

The optical image of Cu@Ni nanoparticles stored for a month is shown in **Figure 32**. It can be seen that, after a month, the Cu@Ni nanoparticles still disperses in PAO6 uniformly, no obvious sedimentation behavior is observed, which is crucial for the application of nanoparticles.

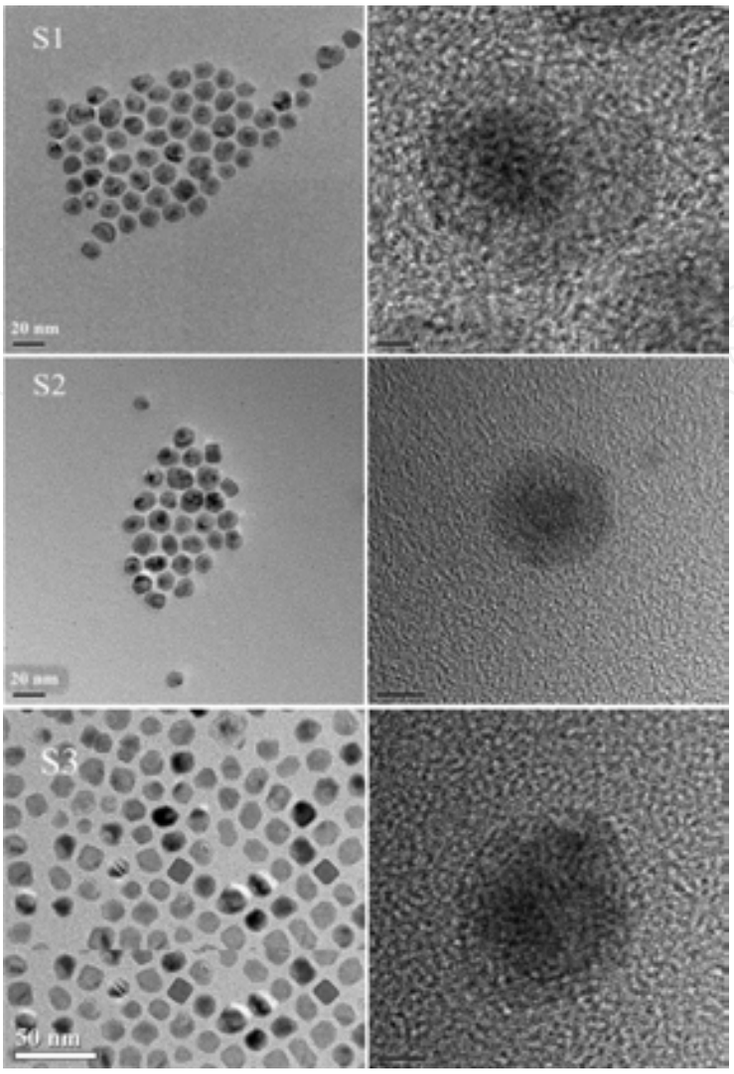

Figure 31. TEM images of surface-capped Cu@Ni nanoparticles with different content of Cu.

Figure 32. Photograph of the Cu@Ni nanoparticles stored in PAO6 after one month.

http://dx.doi.org/10.5772/64592

In order to further study the interaction between organic modifier and inorganic particles of Cu@Ni, FTIR is performed to analyze the modified Cu@Ni nanoparticles, pure OAM and OA. As shown in **Figure 33**, the characteristic peaks at 1711 and 939 cm^{-1} corresponds to the stretching vibration of C═O and bending vibration of ─OH, respectively, in pure OA. As for OAM, the amine absorption peaks at 3367 and 3295 cm^{-1} corresponds to the symmetric and asymmetric stretching vibration of primary amine N-H, peaks at 1583 and 967 cm^{-1} corresponds to the shear mode and bending vibration modes of ─NH2 [27]. For pure OAM and OA, characteristic peaks of nonpolar chain at 2922 and 2852 cm^{-1} are observed, bending vibration of C─H at 1464 cm^{-1} and rocking vibration of not less than four consecutive methylene at 720 cm^{-1} is also observed. For surface-modified Cu@Ni nanoparticles, the existence of nonpolar chain in surface modifiers can be certified through the presence of characteristic peak at 2922, 2852, 1464, and 720 cm^{-1}. At the same time, characteristic peaks of primary amine at 3367, 3295, 1583, and 967 cm^{-1} and the free carboxyl group at 1711 and 939 cm^{-1} is not observed, while the asymmetry and symmetry stretching vibration of ─COO─ peak at 1543 and 1460 cm^{-1} and stretching vibration of C─N at 1071 cm^{-1} appears [28]. It can be concluded reasonably that the interaction between organic surface modifiers and Cu@Ni nanoparticles is a kind of chemical combination, which is essentially different from surface wetting of general dispersant. Because of the more stable chemical coating, oxidation and agglomeration of Cu@Ni particles is effectively prevented, and the nonpolar chain can improve its compatibility with base oil.

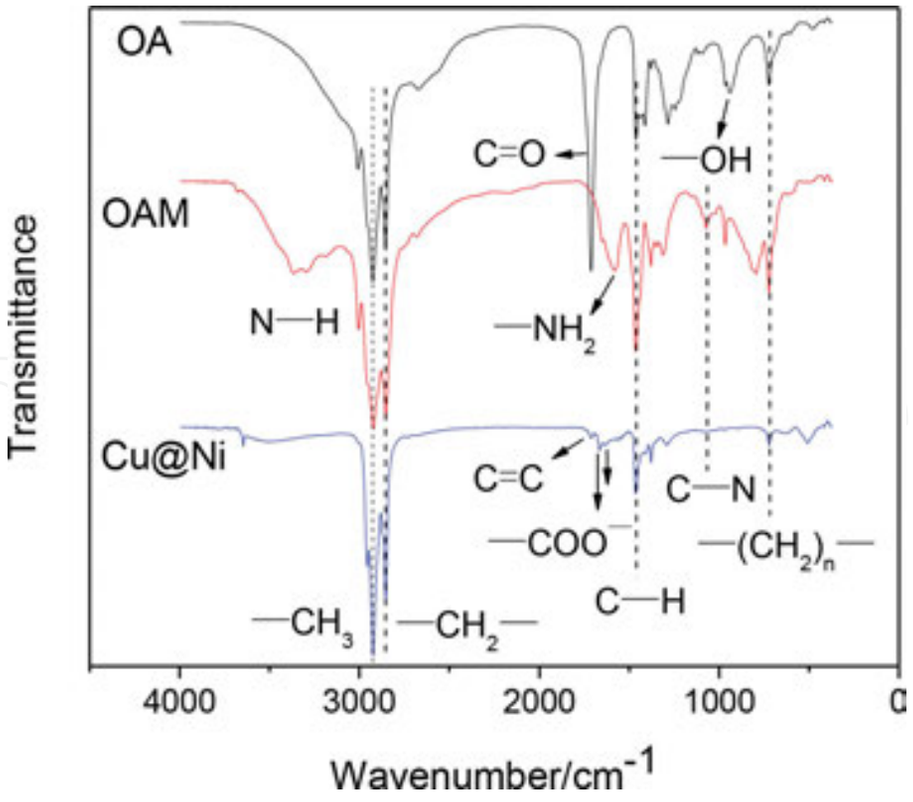

Figure 33. FTIR spectra of OA, OAM, and as-separated Cu@Ni nanoparticles.

The coefficient of friction (COF) (a) and wear scar diameter (WSD) (b) with different Cu@Ni nanoparticles (here represented by S2) concentration is shown in **Figure 34** (four ball machine, 300 N, 1450 rpm, 30 minutes; at the same time data of PAO6 and PAO6 only containing modifier are also given). As can be seen, compared with base oil PAO6, the coefficient of friction of surface modifier increased, but the wear scar diameter is greatly reduced. COF and WSD of Cu@Ni nanoparticles decrease significantly compared with surface modification agent, especially antiwear ability of it in the experimental concentration range. Compared with PAO6, the wear scar diameter of Cu@Ni nanoparticles decrease by 42.6% with mass fraction of 0.025%, by 47.5% with mass frication of 0.80%. In the last chapter, under the lubrication of Ni nanolubricant, the wear scar diameter reduced by 30%. As a result, compared with Ni nanoparticles, the antiwear ability of Cu@Ni composite nanoparticles increases by 17.5%. Therefore, it can be concluded reasonably that because of the synergistic effect of Ni and Cu lubricating and self-repairing film deposited on friction pair avoids direct contact between the interface friction, delays the adhesive wear and timely repairs worn parts, and greatly improves the antiwear ability of base oil PAO6.

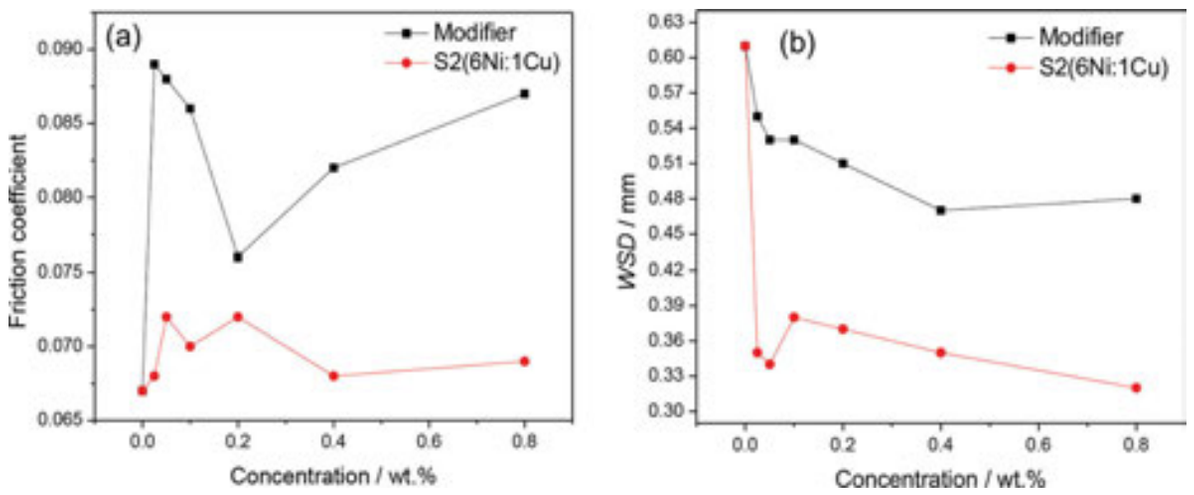

Figure 34. Variation of friction coefficient (a) and wear scar diameter (b) with the concentration of Cu@Ni nanoparticles.

The COF (a) and WSD (b) of PAO6, PAO6 containing only modifiers, and PAO6 containing 0.8% Cu@Ni nanoparticle versus load are shown in **Figure 35** (four ball machine, 1450 rpm, 30 minutes; at the same time, that of PAO6 lubricant containing Ni nanoparticles surface modified under the same condition is also given for comparison). It can be seen that with the increasing of load, COF of Cu@Ni nanoparticles decreases rapidly, and WSD increases slowly. COF of other lubrication conditions sharply decreases at first and then increases WSD. In addition, overall the COF and WSD of Cu@Ni nanoparticles decreases greatly compared to the rest of the lubrication conditions, especially under the load of 400 N, which reveals once again that the Cu@Ni composite nanoparticles has better antifriction, antiwear, and bearing performance than Ni nanoparticles, which may be due to the formation of boundary lubricating film on the sliding surface of the steel ball because of the synergistic action of Ni and Cu.

http://dx.doi.org/10.5772/64592

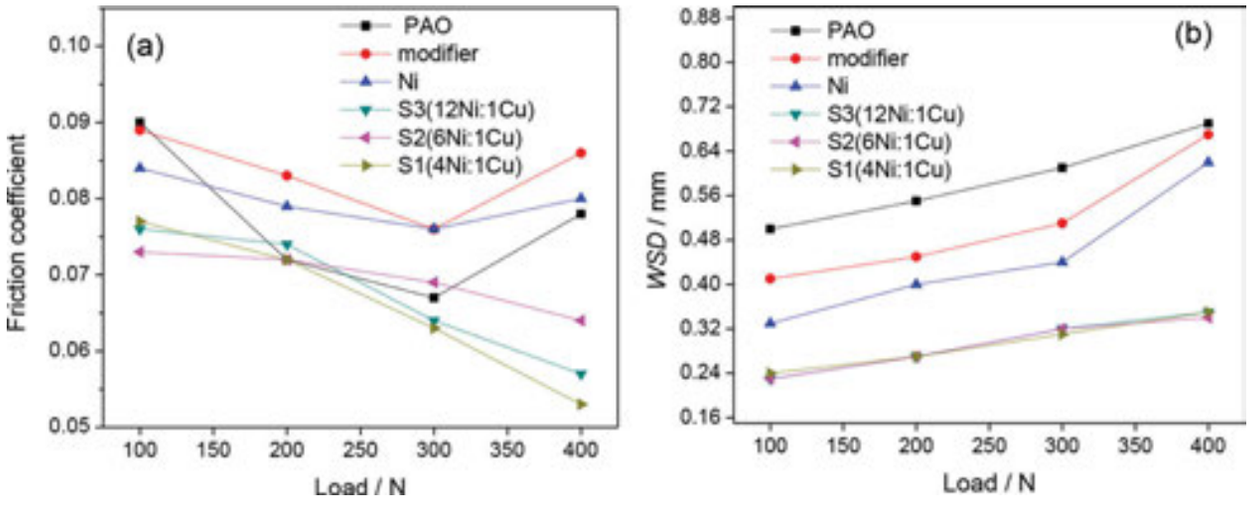

Figure 35. Friction coefficient (a) and wear scar diameter (b) versus applied load under the lubrication of PAO6, PAO6 + surface-modiffiers, and nanolubricants containing 0.8% Cu@Ni nanoparticles with different content of Cu.

P_B(a) and P_D (b) value of PAO6, PAO6 containing only modifiers, and PAO6 containing Cu@Ni nanoparticle are given in **Figure 36** (that of PAO6 containing Ni nanoparticles is also given for comparison). As shown in **Figure 36**, $P_B$of Cu@Ni nanoparticles is obviously higher than that of PAO6 and PAO6 containing only modifiers, however, is similar with that of Ni nanoparticle. For the P_D of all lubricants, Cu@Ni nanoparticles shows the highest values compared with the rest of the lubricants (see **Figure 36 b**). Once again, it is proved that Cu@Ni nanoparticles can effectively ameliorate the extreme pressure ability of PAO6.

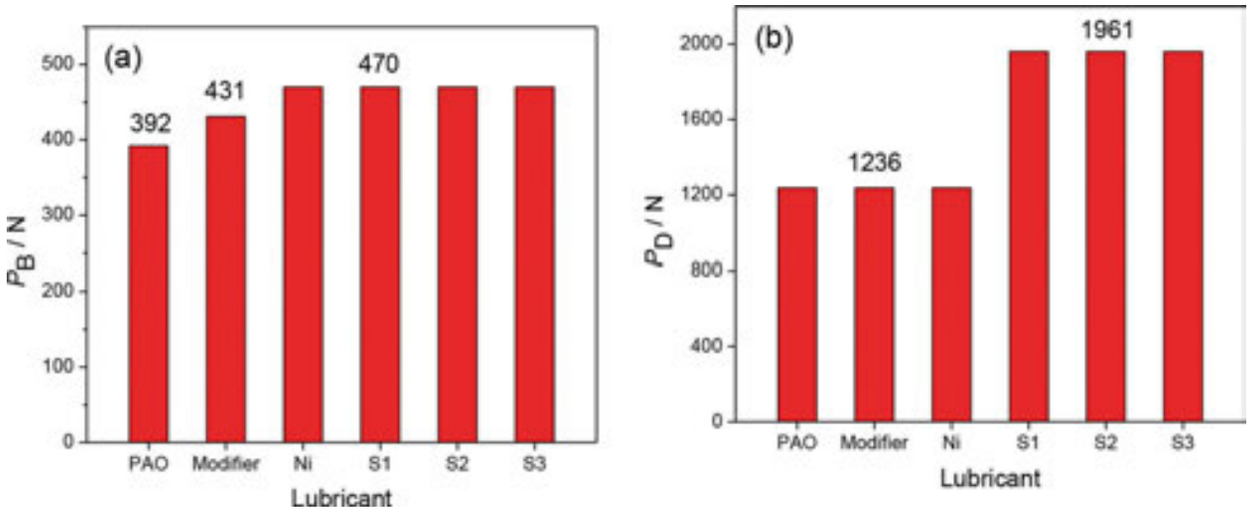

Figure 36. P_B (a) and P_D (b) values of various lubricant systems.

The SEM images of worn surface on steel ball under the three lubrication conditions are shown in **Figure 37** (partial enlarged details are given). It can be seen that the WSD of steel ball lubricated by Cu@Ni of nanoparticles is obviously less than that of pure PAO6 and PAO6 containing modifier, and the worn surface is smooth with minor scratches. For PAO6, obvious

scratches and adhesion wear is observed, which once again proves that the Cu@Ni nanoparticles shows better antiwear performance.

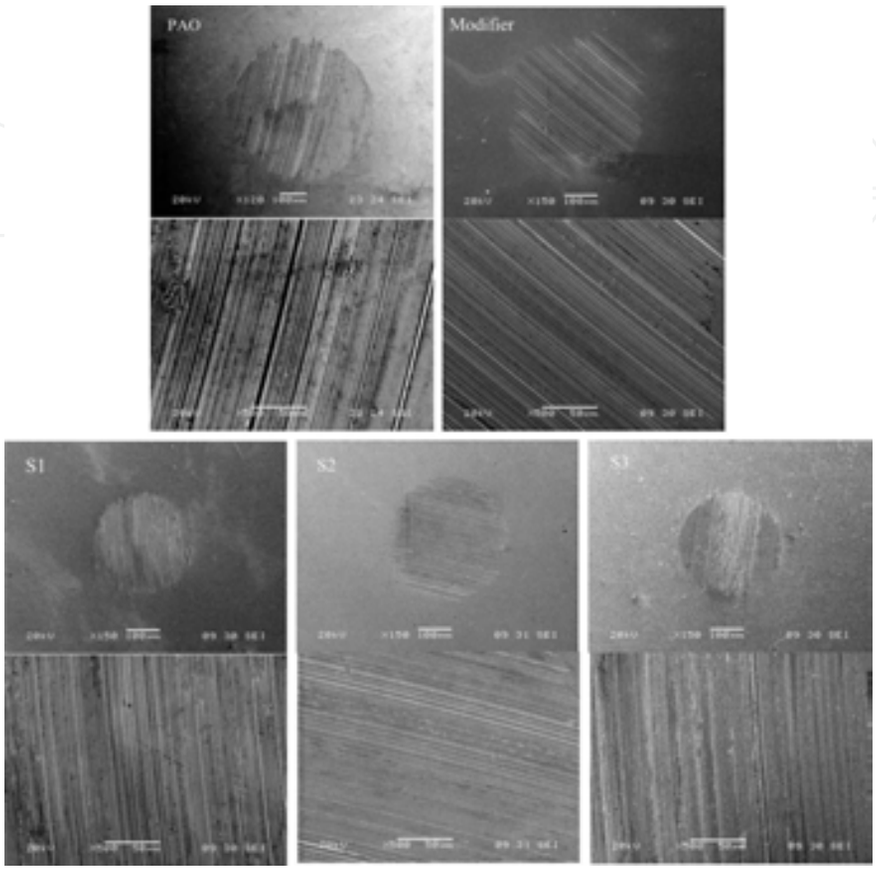

Figure 37. SEM micrographs of wear scars lubricated with PAO6 as well as PAO6 + surface-modifiers and nanolubricants containing 0.8% Cu@Ni nanoparticles.

In order to reveal the antifriction and antiwear mechanism of Cu@Ni nanoparticles, XPS is used to analyze the chemical state of several typical elements on worn surface of steel ball. **Figure 38** shows the curve-fitted XPS spectra of C 1s, O 1s, N 1s, Fe 2p, Ni 2p, and Cu 2p on wear scar surface under the lubrication conditions of PAO6 with 0.8% Cu@Ni nanoparticles (S2) (four ball mode, 1450 rpm and 400 N, 30 minutes). It can be noticed that O, N elements are detected which come from surface modifiers containing C—N, COO—, C═C, and C—H absorbed or reacted with worn surface of steel ball. The Fe 2p3/2 peak at 710.81 eV (corresponding satellite peak is located at 713.00 eV) is attributed to Fe_2O_3 (corresponding O 1s peak is located at 529.99 eV) [31]. We can therefore reasonably conclude that ferrous oxides are formed on the worn surfaces of steel balls under selected experimental conditions. Moreover, Ni 2p3/2 peak at 855.94 eV and Ni 2p1/2 peak at 873.64 eV indicate that Ni nanocores can be released from surface-modified Ni nanoparticles and transfers onto sliding steel surface during the rubbing process. Furthermore, a part of Ni nanocores can react with oxygen to form Ni_2O_3 (corresponding O 1s peak is located at 531.66 eV). Moreover, Cu 2p3/2 peak at 932.90 eV

http://dx.doi.org/10.5772/64592

and Cu 2p1/2 peak at 953.05 eV indicate that metal Cu released from Cu@Ni nanoparticles transfers to the worn surface of steel ball, from which it can be concluded that the synergistic effect of Cu nanoparticles with self-repairing performance and Ni nanoparticles with high activity results in forming boundary lubricating film covering sliding surface during friction process, thus showing better tribological properties.

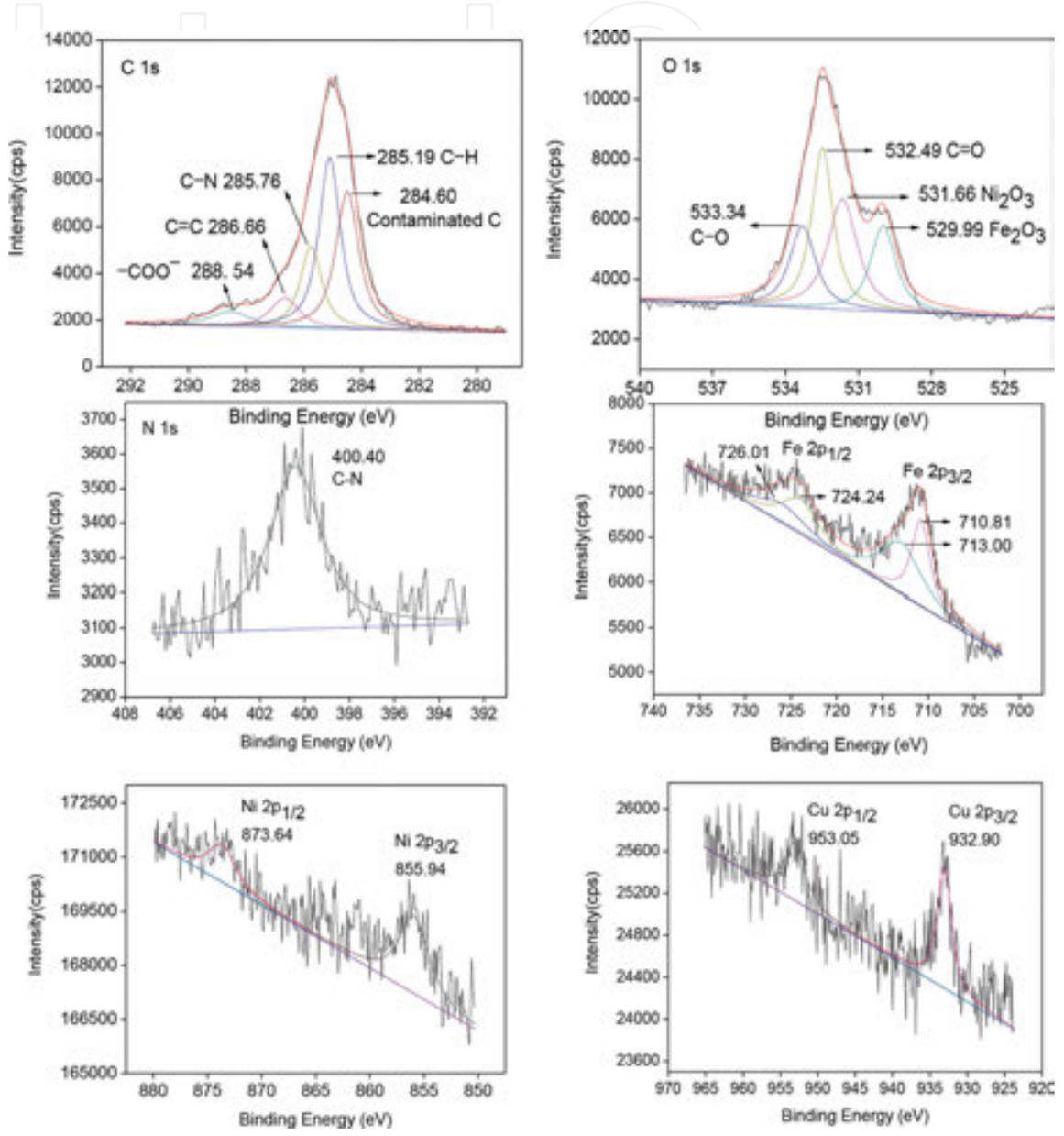

Figure 38. Curve-fitted XPS spectra of typical elements on rubbed surface of steel ball lubricated with nanolubricants containing 0.8% CuNi(S2).

According to the XPS analysis it can be inferred that during the direct contact sliding process, tribochemical reaction occurs between Cu@Ni nanoparticles and steel ball, in which organic modifiers and Ni, Cu nanocores with high activity are released and transferred to worn surface easily to form continuous and uniform boundary lubricating film. Especially under the

synergistic effect of Ni and Cu nanoparticles, an antifriction and self-repairing film deposited on friction pair can reduce direct contact between sliding surface, delay adhesion wear, and timely repair wear parts, thus greatly improving the antifriction, antiwear, and extreme pressure performance of PAO.

6. Conclusion

In this chapter, nano-Ni and the Cu@Ni nanoparticles with different size and shape are prepared through *in situ* thermal decomposition. Their properties as additives in base oil and DLC solid-liquid composite lubrication system are systematically studied. It was found that Ni and Cu@Ni nanoparticles showed outstanding antifriction and antiwear properties in base oil and DLC solid-liquid composite lubrication system. And the size and shape of nanoparticles affects their tribological properties greatly. The results are as follows:

1. Ni nanoparticles with three type of particle size can significantly improve the wear resistance as lubricating oil additives, and its wear resistance is closely related to particle size. The smaller the particle size is, the better the wear resistance is. When Wt 0.05% Ni particle was added in base oil, the WSD of steel ball can be reduced by 30%.
2. Nano-Ni particles with three different morphologies including triangular rod, triangular plate, and spherical shape were added in lubricating oil. Triangle sheet-like Ni nanoparticles' performance is better than the other ones due to its larger contacting area with steel ball. The WSD of steel ball can be reduced by 35%.
3. The Ni nanoparticles (7 nm diameter) significantly reduce the friction in the DLC/steel contacts lubricated by fully formulated oil di-iso-octyl sebacate (DIOS) in all the lubrication regimes: boundary, mixed, and elasto-hydrodynamic lubrication.
4. Compared with pure Ni nanolubricant, Cu@Ni nanolubricant shows better antimill, friction reduction, and bearing capacity. The antiwear capacity is enhanced by 17.5%. The mechanism can be deduced that the collaborative work of Ni nuclear deposition film and Cu transfer film can effectively reduce direct contact between friction interface and timely repair wear parts.

Author details

Yujuan Zhang, Shengmao Zhang*, Pingyu Zhang, Guangbin Yang and Zhijun Zhang

*Address all correspondence to: zsm@henu.edu.cn

Engineering Research Center for Nanomaterials, Henan University, Kaifeng, China

Collaborative Innovation Center of Nano Functional Materials and Applications of Henan Province, Henan University, Kaifeng, China

References

[1] Bakunin, V.N., Suslov, A.Y., Kuzmina, G.N., Parenago, O.P., Topchiev, A.V. Synthesis and application of inorganic nano-particles as lubricant components-a review. J. Nanopart. Res. 2004;6:273–284.

[2] Wei Dai, Bassem Kheireddin, Hong Gao, Hong Liang, Roles of nanoparticles in oil lubrication, Tribology internationaly, 2016;102:88–98.

[3] Zhou, J., Wu, Z., Zhang, Z., Liu, W., Xue, Q. Tribological behavior and lubricating mechanism of Cu nanoparticles in oil. Tribol. Lett. 2000;8:213–218.

[4] Tarasov, S., Belyaev, S. Alloying contact zones by metallic nanopowders in sliding wear. Wear. 2004;257:523–530.

[5] Lee, K., Hwang, Y., Cheong, S., Choi, Y., Kwon, L., Lee, J. Understanding the role of nanoparticles in nano-oil lubrication. Tribol. Lett. 2009;35:127–131.

[6] Herna´ndez Battez, A., Viesca, J.L., Gonza´lez, R., Blanco, D., Asedegbega, E., Osorio, A. Friction reduction properties of a CuO nanolubricant used as lubricant for a NiCrBSi coating. Wear. 2010;268:325–328.

[7] Zhang, Z., Zhang, J., Xue, Q. Synthesis and characterization of a molybdenum disulfide nanocluster. J. Phys. Chem. 1994;98:12973–12977.

[8] Zhang, Z., Xue, Q., Zhang, J. Synthesis, structure and lubricating properties of dialkyldithiophosphate-modified Mo-S compound nanoclusters. Wear. 1997;209:8–12.

[9] Xue, Q., Liu, W., Zhang, Z. Friction and wear properties of a surface-modified TiO2 nanoparticle as an additive in liquid paraffin. Wear. 1997;213:29–32.

[10] Zhou, J., Yang, J., Zhang, Z., Liu, W., Xue, Q. Study on the structure and tribological properties of surface-modified Cu nanoparticles. Mater. Res. Bull. 1999;34:1361–1367.

[11] Zhou, J., Wu, Z., Zhang, Z., Liu, W., Dang, H. Study on an antiwear and extreme pressure additive of surface coated LaF3 nanoparticles in liquid paraffin. Wear. 2001;249:333–337.

[12] Dang, H., Sun, L., Zhou, J., Zhang, Z. Synthesis, structure and tribological properties of stearic acid coated (NH4)3PMo12O40 nanoparticles. Tribol. Lett. 2004;17:311–316.

[13] Li, X., Cao, Z., Zhang, Z., Dang, H. Surface-modification in situ of nano-SiO2 and its structure and tribological properties. Appl. Surf. Sci. 2006;252:7856–7861.

[14] Xiong, X., Kang, Y., Yang, G., Zhang, S., Yu, L., Zhang, P. Preparation and evaluation of tribological properties of Cu nanoparticles surface modified by tetradecyl hydroxamic acid. Tribol. Lett. 2012;46:211–220.

[15] Tzitzios, V., Basina, G., Gjoka, M., Alexandrakis, V., Georgakilas, V., Niarchos, D. Chemical synthesis and characterization of hcp Ni nanoparticles. Nanotechnology. 2006;17:3750–3755.

[16] Sun, Y., Rollins, H., Guduru, R. Preparations of nickel, cobalt, and iron nanoparticles through the rapid expansion of supercritical fluid solutions (RESS) and chemical reduction. Chem. Mater. 1999;11:7–9.

[17] Han, M., Liu, Q., He, J., Song, Y., Xu, Z., Zhu, J.M. Controllable synthesis and magnetic properties of cubic and hexagonal phase nickel nanocrystals. Adv. Mater. 2007;19:1096–1100.

[18] Carenco, S., Labouille, S., Bouchonnet, S., Boissie`re, C., Le Goff, X.-F.L. Revisiting the molecular roots of a ubiquitously successful synthesis: nickel(0) nanoparticles by reduction of [Ni(acetylacetonate)2]. Chem. Eur. J. 2012;18:14165–14173.

[19] Carenco, S., Boissie`re, C., Nicole, L., Sanchez, C., Le Floch, P., Me´zailles, N. Controlled design of size-tunable monodisperse nickel nanoparticles. Chem. Mater. 2010;22:1340–1349.

[20] Lu, A.-H., Salabas, E.L., Schüth, F. Magnetic nanoparticles: synthesis, protection, functionalization, and application. Angew. Chem. Int. Edit. 2007;46:1222–1244.

[21] Winnischofer, H., Rocha, T.C.R., Nunes, W.C., Socolovsky, L.M., Knobel, M., Zanchet, D. Chemical synthesis and structural characterization of highly disordered Ni colloidal nanoparticles. ACS Nano. 2008;2:1313–1319.

[22] Chen, Y., Peng, D., Lin, D., Luo, X. Preparation and magnetic properties of nickel nanoparticles via the thermal decomposition of nickel organometallic precursor in alkylamines. Nanotechnology. 2007;18:505703.

[23] Qiu, S., Zhou, Z., Dong, J., Chen, G. Preparation of Ni nanoparticles and evaluation of their tribological performance as potential additives in oils. J. Tribol. 2001;123:441–443.

[24] Chou, R., Battez, A.H., Cabello, J.J., Viesca, J.L., Osorio, A., Sagastume, A. Tribological behavior of polyalphaolefin with the addition of nickel nanoparticles. Tribol. Int. 2010;43:2327–2332.

[25] Liang, X., Wang, X., Zhuang, J., Chen, Y., Wang, D., Li, Y. Synthesis of nearly monodisperse iron oxide and oxyhydroxide nanocrystals. Adv. Funct. Mater. 2006;16:1805–1813.

[26] Sun, S., Zeng, H., Robinson, D.B., Raoux, S., Rice, P.M., Wang, S., Li, G. Monodisperse MFe2O4 (M = Fe, Co., Mn) nanoparticles. J. Am. Chem. Soc. 2004;126:273–279.

[27] Li, N., Zhang, X., Chen, S., Hou, X., Liu, Y., Zhai, X. Synthesis and optical properties of CdS nanorods and CdSe nanocrystals using oleylamine as both solvent and stabilizer. Mater. Sci. Eng. B. 2011;176:688–691.

[28] Shukla, N., Liu, C., Jones, P.M., Weller, D. FTIR study of surfactant bonding to FePt nanoparticles. J. Magn. Magn. Mater. 2003;266:178–184.

[29] Söderlind, F., Pedersen, H., Petoral, R.M., Käll, P.-O., Uvdal, K. Synthesis and characterisation of Gd2O3 nanocrystals functionalised by organic acids. J. Colloid Interface Sci. 2005;288:140–148.

[30] Shah, F.U., Glavatskih, S., Antzutkin, O.N. Synthesis, physicochemical, and tribological characterization of S-Di-n-octoxyboron-O, O′-di-n-octyldithiophosphate. ACS Appl. Mater. Interfaces. 2009;1:2835–2842.

[31] Wang, L., Gao, Y., Xu, T., Xue, Q. A comparative study on the tribological behavior of nanocrystalline nickel and cobalt coatings correlated with grain size and phase structure. Mater. Chem. Phys. 2006;99:96–103.

[32] Cai, M., Liang, Y., Zhou, F., Liu, W. Tribological properties of novel imidazolium ionic liquids bearing benzotriazole group as the antiwear/anticorrosion additive in poly(ethylene glycol) and polyurea grease for steel/steel contacts. ACS Appl. Mater. Interfaces. 2011;3:4580–4592.

[33] Bradley, J.S., Tesche, B., Busser, W. Surface spectroscopic study of the stabilization mechanism for shape-selectively synthesized nanostructured transition metal colloids. J. Am. Chem. Soc. 2000;122:4631–4636.

[34] Yamamoto, T., Yin, H., Wada, Y. Morphology-control in microwave-assisted synthesis of silver particles in aqueous solutions. Bull. Chem. Soc. 2004;77:757–761.

[35] Wang, F., Zhang, Z.C., Chang, Z.Q. Effects of magnetic field on the morphology of nickel nanocrystals prepared by gamma-irradiation in aqueous solutions. Mater. Lett. 2002;55(1–2):27–29.

[36] Zhang, C., Zhang, S., Yu, L. Size-controlled synthesis of monodisperse Ag_2S nanoparticles by a solventless thermolytic method. Mater. Lett. 2012;85:77–80.

[37] Ronkainen, H., Varjus, S., Holmberg, K. Friction and wear properties in dry, water-and oil-lubricated DLC against alumina and DLC against steel contacts. Wear. 1998;222(2): 120–128.

[38] Miklozic, K.T., Lockwood, F., Spikes, H. Behaviour of boundary lubricating additives on DLC coatings. Wear. 2008;265(11–12):1893–1901.

[39] Kalin, M., Viintin, J. A comparison of the tribological behaviour of steel/steel, steel/DLC and DLC/DLC contacts when lubricated with mineral and biodegradable oils. Wear. 2006;261(1):22–31.

[40] Jia, Z., Xia, Y., Li, J. Friction and wear behavior of diamond-like carbon coating on plasma nitrided mild steel under boundary lubrication. Tribol. Intl. 2010;43(1–2):474–478.

[41] Sanche-Lopez, J.C., Erdemir, A., Donnet, C. Friction-induced structural transformations of diamond like carbon coatings under various atmospheres. Surf. Coat. Tech. 2003;163–164:444–450.

[42] Kalin, M., Viintin, J. Real contact temperatures as the criteria for the reactivity of diamond-like carbon coatings with oil additives. Thin Solid Films. 2010;518(8):2029–2036.

[43] Neville, A., Morina, A., Haque, T., Voong, M. Compatibility between tribological surfaces and lubricant additives—how friction and wear reduction can be controlled by surface/lube synergies. Tribol. Intl. 2007;40(10–12):1680–1695.

[44] Haque, T., Morina, A., Neville, A., Kapadia, R., Arrowsmith, S. Study of the ZDDP antiwear tribofilm formed on the carbon coating using AFM and XPS. J. ASTM Intl. 2007;4(11):http://dx.doi.org/10.1520/JAI100937.

[45] Kalin, M., Kogovšek, J., Remškar, M. Nanoparticles as novel lubricating additivesin a green, physically based lubrication technology for carbon coatings. Wear. 2013;303:480–485.

[46] Ghaednia, H., Babaei, H., Jackson, R.L., Bozack, M.J., Khodadadi, J.M. The effect of nanoparticles on thin film elasto-hydrodynamic lubrication. Appl. Phys. Lett. 2013;103:263111.

[47] Liu, Y., Erdemir, A., Meletis, E.I. A study of the wear mechanism of diamond-like carbon films. Surface Coatings Technol. 1996;82(1–2):48–56.

[48] Liu, Y., Erdemir, A., Meletis, E.I. An investigation of relationship between graphitization and frictional behavior of DLC coatings. Surface Coatings Technol. 1996;86–87(1–3):564–568.

[49] Erdemir, A., Bindal, C., Fenske, G.R. Characterization of transfer layers forming on surface sliding against diamond-like carbon. Surface Coatings Technol. 1996;86–87:692–697.

[50] Kogovšek, J., Remškar, M., Kalin, M. Lubrication of DLC-coated surfaces with MoS2 nanotubes in all lubrication regimes: Surface roughness and running-in effects. Wear. 2013;303:361–370.

[51] Gelinck, E.R.M., Schipper, D.J. Calculation of Stribeck curves for line contacts. Tribol. Intl. 2000;33:175–181.

[52] Huang, P. Physical-mathematical model and numerical analysis of nano thin film lubrication. Tribology. 2003;23(1):60–64.

[53] Kalin, M., Velkavrh, I. Non-conventional inverse-Stribeck-curve behaviour and other characteristics of DLC coatings in all lubrication regimes. Wear. 2013;297:911–918.

[54] Wang, W.Z., Huang, P. Study on the lubrication state of frictional pairs with different surface roughness based on Stribeck curves. Tribology. 2004;24(3):254–257.

[55] Nilsson, D., Prakash, B. Influence of different surface modification technologies on friction of conformal tribopair in mixed and boundary lubrication regimes. Wear. 2011;273:75–81.

[56] Chen, S., Sommers, J.M. Alkanethiolate-protected copper nanoparticles: spectroscopy, electroche-mistry, and solid-state morphological evolution. J. Phys. Chem. B. 2001;105:8816–8820.

[57] Engels, V., Benaskar, F., Jefferson, D.A. Nanoparticulate copper-routes towards oxidative stability. Dalton T. 2010;39:6496–9502.

[58] Tsarfati, T., Zoethout, E., Bijkerk, F. Growth and sacrificial oxidation of transition metal nanolayers. Surf. Sci. 2009;603:1041–1045.

[59] Honkanen, M., Vippola, M., Lepisto, T. Oxidation of copper alloys studied by analytical transmission electron microscopy cross-sectional specimens. J. Mater. Res. 2008;23(5): 1350–1357.

[60] Guo, H., Chen, Y., Ping, H. One-pot synthesis of hexagonal and triangular nickel-copper alloy nanoplates and their magnetic and catalytic properties. J. Mater. Chem. 2012;22:8336–8344.

[61] Zhang, S., Zeng, H. Solution-based epitaxial growth of magnetically responsive Cu@Ni nanowires. Chem. Mater. 2010;22:1282–1284.

IntechOpen